



Politecnico di Torino

FACOLTÀ DI INGEGNERIA

Corso di Laurea Magistrale in Ingegneria Matematica

**TESI DI LAUREA
MAGISTRALE**

**Mathematical modelling of how the mechanical
properties of a host tissue affect tumours kinetics
and dynamics**

Candidato:
Elena Sofia D'Ambrosio
Matricola 241669

Relatore:
Luigi Preziosi
Helen Byrne

Anno Accademico 2018–2019

Contents

1	Introduction	5
2	Multiphase Models	17
2.1	Mass and momentum balances	17
2.2	Characterization of Phases Stress Tensors	19
2.3	Momentum Balances Reformulation	23
2.4	The surrounding medium	25
3	Mathematical Model	29
3.1	Physical description of Chen et al. Model [2]	29
3.2	Introduction to the model	29
3.3	Chen et al. [2] model	30
3.4	Non-Necrotic Model	32
3.5	Necrotic Model	34
3.6	Non-dimensional Model	35
4	Computation of the solution for the tumour model	39
4.1	Proliferative Phase	40
4.2	Apoptosis and Necrotic Phase	41
5	Analysis and simulations	45
5.1	Proliferative phase	45
5.2	Apoptosis Phase	46
5.3	Apoptosis phase with the onset of necrosis	55

Chapter 1

Introduction

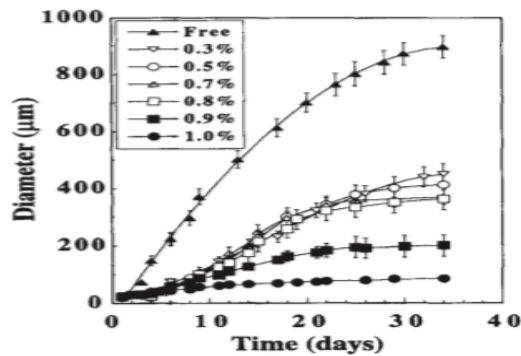
Tumours can arise from cells which belong to every kind of tissue and their different origins determine specific structured appearances. Their birth can be attributed to neoplasms, abnormal tissue masses where control mechanisms become deficient, and cells proliferation exceed without any correlation with normal growth or tissue repair. The neoplasm consists of tumour cells and also some blood vessels and supporting stroma. The abnormal rate of cells proliferation can vary from slightly above normal proliferative thresholds to uncontrolled levels of growth which may cause the subsequent neoplasm extension into the adjacent tissues.

Tumours can be divided into two main categories [4]: benign and malignant, which represent the extremes of a spectrum of different behaviours that can arise. In general, benign tumours are characterized by uniform cell shapes, slow growth, no invasion of adjacent tissues or metastasis, high differentiation. On the other hand, malignant tumours may exhibit less grade of differentiation (how much or how little tumour tissue resembles the normal tissue it came from), differences in cell growth and shapes, invade the surrounding tissues and spread to other tissues via metastasis. We can identify three main ways in which benign tumours differ from malignant ones: their degree of differentiation, their rate of growth and how they grow. However, we can distinguish two distinct phases in solid tumour growth: avascular and vascular. The transition from one stage to another is made through the secretion of chemical compounds called 'tumour angiogenesis factor' by the solid tumour into the host tissue. TAF stimulates the growth of new capillary vessels from the host's pre-existing vessels [7], which ensures consequent nutrition and progression to the vascular phase, where rapid growth and invasion of the surrounding healthy tissue may occur.

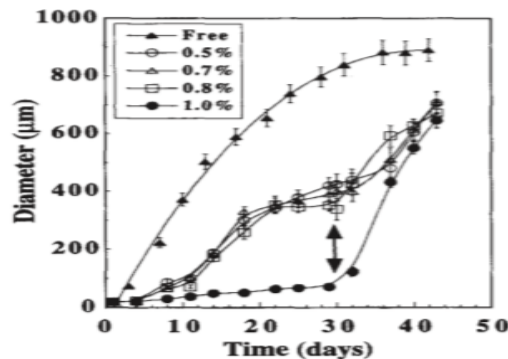
For this reason, understanding of the avascular phase is important to prevent further development of the tumour. When avascular tumours are prevented from obtaining nutrition through an adjacent blood supply, they obtain vital nutrients and growth factors via diffusion from the neighboring environment. If they do not enter the vascular phase, they start a dormant period. Tumour dormancy may be characterised by a balance between actively proliferating cells and cells undergoing apoptosis. Consequent aggressive growth may be then due not to an increase in the proliferative rate, but a decrease of the apoptotic rate. Such a reduction in the rate of cell apoptosis has been hypothesized to be caused by the solid stress imposed by an extracellular matrix or the surrounding tissue,

which limits tumour growth. Growth inhibition might occur via a stress-imposed increase in the rate of accumulation of viable cells in the quiescent state.

In normal tissues the processes of growth, remodelling and morphogenesis are strongly correlated with the stress field. Helmlinger et al. (1997) demonstrated that solid stress suppresses tumour growth in vitro regardless of host species, the tissue of origin or differentiation state. They grew tumour spheroids in agarose gel of different concentrations, regarding the gel as a poro-elastic material. A particular focus was also posed on how the stress macroscopic growth inhibition affects the stress-induced changes in cellular parameters. Two different approaches were employed. The first one was the following.



(a) Comparison between gel-embedded spheroids with free-suspension spheroids in the diameters growth vs. time.



(b) Comparison between gel-embedded spheroids with free-suspension spheroids in the diameters growth vs. time before-after gel release.

Figure 1.1: Growth kinetics of LS174T spheroids. [1]

The growth kinetics of tumour spheroids has been seen to follow the Gompertz law, an empirical relation for volume growth:

$$\ln \left(\ln \left(\frac{V}{V_0} \right) \right) = -\alpha t + \frac{V_{max}}{V_0},$$

where V is a measure estimation of spheroid size, V_0 is the initial size and V_{max} is the final one. The scalar parameter α can be seen as the proliferation rate of cells in the proliferative pool for two compartments experiments (proliferative vs. nonproliferative cells). Values of the α parameter were obtained by plotting the

growth curves (fig.1.1) as $\ln\left(\ln\left(\frac{V}{V_0}\right)\right)$ vs. $-\alpha t$: data were best approximated by single linear fits. For LS174 spheroids identical values of α were obtained for 0,3%-to-1% gel concentrations and also for free suspensions. Similar results were detected when releasing spheroids from the gel, and free-suspension growth resumed. For this reason, we can infer that the imposed solid stress even if affects the macroscopic tumour growth, does not make significant changes in the net proliferation rate when compared with free suspensions.

Another approach to quantify the difference of cell proliferation and apoptosis in plateau-phase LS174T spheroids cultured in free suspension and gels was to use PCNA and TUNEL assays (an investigative procedure which exploits an enzyme that catalyzes attachment of deoxynucleotides, tagged with a fluorochrome or another marker [8]). Positive PCNA staining was applied to outermost cell layers of spheroids; on the contrary, apoptosis was examined only in the central parts. The main difference between spheroids cultured in free-suspension and those cultured in a gel was the presence of large voids in the inner regions attributed to necrosis: large voids were frequently spotted in free suspension spheroids, contrarily in gel-cultured ones in which they were rarely detected. The experiments were conducted by dividing the spheroids into two distinct groups depending on their sizes: small ($D < 300\mu m$) vs. large spheroids ($D > 300\mu m$). Bold bars in (a) and (b) of fig. (1.4) can be used to testify the rates behaviours: in (a) the slope of bold bars is 0 for both spheroids grown in the free suspension and 0,7% gel; while it is positive in (b) for free suspension and 0 for gels. We can thus infer that there was no size correlation for the PCNA data for both the analysed scenarios; instead, the percentage of TUNEL cells experienced an increase with size in free suspensions spheroids, but not in 0,7%-gel spheroids. Exploiting the size dependence as an estimation of the previous rates, we can then affirm that solid stress did not affect the proliferative rate (as already shown in the Gompertz approach), but decreased the apoptotic rate seen the difference between 0,7% gels and free-suspension scenarios. As already stated previously, such a decrease leads to an accumulation of quiescent cells, causing the augment of packing cell density values, as it can be seen in fig. (1.5).

To conclude, these plateau-phase stressed spheroids displayed simultaneously, at a cellular level, a reduction in the apoptotic rate, negligible necrosis, and a similar proliferation rate when compared with the free-suspension cultured spheroids. Given the simultaneous decrease in the apoptotic rate and the increase in cellular density, we can then infer that stress-induced inhibition of macroscopic tumour growth gives the tumour a survival advantage. Cell-Cell interactions, which are presumably reinforced at higher cell densities, contributed to inhibiting cell death. Increased cell density and the subsequently strengthened compaction, generated by external stress, can be considered the pioneers of a multicellular-dependent mechanism of amplified radiation resistance and both intrinsic and acquired drug resistance. In fact, chemical signals do not represent the only regulators of tissue development and cells behaviour, but, also, physical signals become crucial in their regulation. Since cells are constantly experiencing forces, they have developed mechanical response sensors, molecules which convert physical stimuli into a biochemical signal.

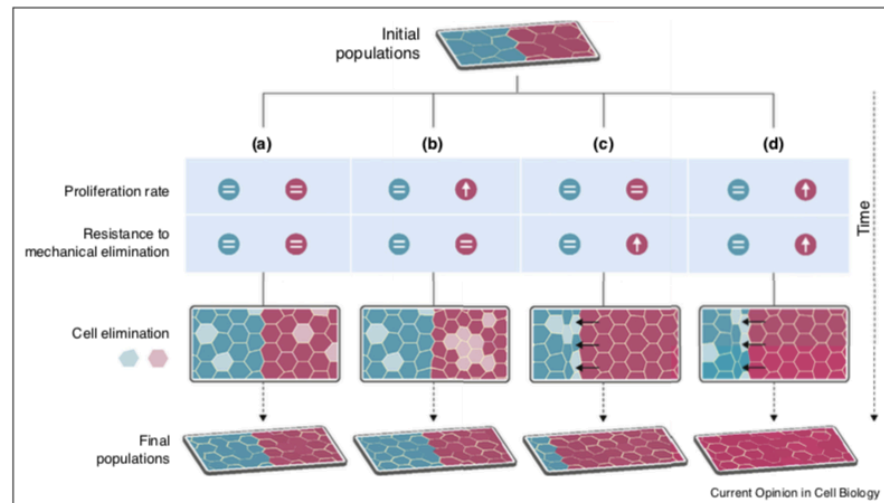
Biological processes such as cell proliferation, differentiation and migration

are crucially modulated by mechano-transduction; in fact, alterations in forces or inadequate cellular response to those forces lead to developmental defects and diseases like atherosclerosis and cancer [9].

Tissues carry the ability to quantify cell density and to model and grow by the constraints imposed by the available space. Cells, to avoid tissue-overcrowding, can sense the surrounding mechanical cues, as well as microenvironmental external properties, such as rates of proliferation and accordingly shape their behaviour. Therefore, to guarantee tissue homeostasis, a balance between cell cycle regulation and cell elimination must be kept.

In 2005, Shraiman [10] suggested for the first time that mechanical interactions could influence tissue growth and cell competition. Experiments in which the total available space is restricted were conducted with cells having different proliferative rates and resistance to mechanical elimination. It has been shown that a hallmark for being the winner population is displaying less sensitiveness to mechanical elimination, which ensures the fast-growing cells with such skill to easily expand by compressing the loser population (fig. (1.2)).

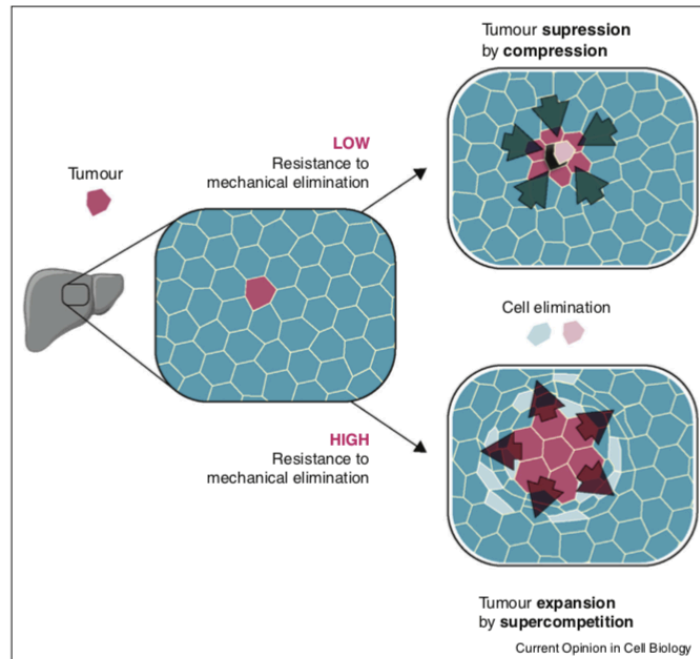
Competition for space is also evident in a tumour microenvironment. The tumour, to expand, needs not only to overcome the compressive stress exerted by the surrounding tissue but also the growth inhibitory mechanical feedback activated by its high growth rate. Below it is shown how the degree of resistance of wild type (WT) cells affect the tumour expansion (fig. (1.3)).



Impact of differential proliferation rate and resistance to mechanical elimination during tissue development, if cells respect space constraints and the epithelium remains flat. **(a)** A proliferative tissue suffers a homogeneous increase in cell density due to a uniform proliferation rate and ability to resist to mechanical-induced elimination. In this situation, competition for the available space is not detected and cells are eliminated randomly. **(b)** When cells have the same sensitivity to deformation and survive equally to mechanical-induced elimination, but have different proliferation rates, tension builds up in the centre of the fast-proliferative population. As a result, these cells subjected to higher compression stress arrest their cell cycle and eventually are eliminated, to restore homogenous tissue growth. **(c)** The resistance to deformation and mechanical-induced elimination is sufficient to provide a competitive advantage. As cells proliferate, the cell density increases uniformly. Then, cells that are less sensitive to compaction and thus are more resistant to compression-promoted elimination, compress and trigger elimination of adjacent cells. Accordingly, hypersensitivity to crowding may represent a hallmark of loser status. Nevertheless, the expansion of the mechanical winner cells is slower than if they also had a proliferative advantage. **(d)** When fast-proliferative cells display a higher resistance to mechanical-induced elimination, the pressure created is felt by the adjacent cells. Compressive stress deforms the slow-proliferative cells, causing their elimination. This way the fast-proliferative cells keep expanding, colonizing the entire tissue at the expenses of the mechanical-unfit cells. Arrows indicate the direction of the compression stress. Light cells correspond to eliminated cells.

Figure 1.2: Impact of differential proliferation rate and resistance to mechanical elimination during tissue development. [9]

Further experiments on stress-induced inhibition of tumour growth were con-



Mechanical cell competition in cancer. Tumour cells (purple) arise frequently in organs. Their elimination or expansion depend on their relative resistance to mechanical elimination in comparison to the surrounding WT cells. When tumour cells display hypersensitivity to compaction, cell competition acts as a tumour suppression mechanism, promoting the removal of those dangerous cells. Here compression of the tumour cells by the adjacent WT cells triggers their elimination. Nonetheless, cell competition can act as a tumour expansion mechanism through a process called supercompetition. Acquisition of survival advantage, a hallmark of cancer, by the tumour cells sustains their ability to keep proliferating and expand. A higher sensitivity to compaction of the WT surrounding cells allows tumour cells to promote their elimination, upon compression. The resistance to mechanical-induced elimination may work as a ruling hallmark of mechanical supercompetition, since is sufficient to explain tumour progression and invasion of the surrounding WT tissue. Arrows indicate the direction of the compression stress. Light cells correspond to eliminated cells.

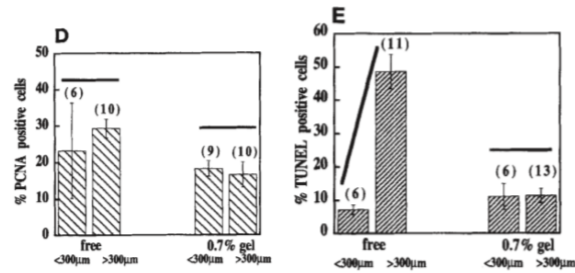
Figure 1.3: Mechanical cell competition in cancer [9]

ducted by Cheng et al. in 2009.

In Cheng et al. study [5], they used embedded fluorescent micro-beads as strain markers in agarose gel and monitored their relative displacements to estimate the strain and related the corresponding accumulating mechanical stress in the gel which surrounded non-metastatic murine carcinoma 67NR tumour spheroids. Agarose gels are frequently utilised in tumour experiments for their resistance to cancer cells proteinases, make it thus possible to study the solid stress regardless of cell invasion. In their tests, growing spheroids progressively compressed the surrounding gel, as revealed by 3D confocal microscopy. By the day 30, as shown in the following pictures (fig.1.6), spheroids diameter had attained $\sim 250\mu\text{m}$ and ρ_{beads} (micro-beads density) in the first $10\mu\text{m}$ -thick shell of agarose gel was $\sim 1,6$ times greater than the unstressed cases.

It has been shown, however, that there is a strong correlation between the structure of the imposed stress and the shape of growing spheroids. The micro-beads density increase accounts for not only the variation of gel's strain but also the organization of the peri-stress field around spheroids edges. The general tendency of the tumour spheroids is to expand in the direction of less stress (where the micro-beads are less concentrated, fig. 1.7); thus allowing the geometry transition to elongated-shape aggregates.

According to Helmlinger experiments, Cheng. et al. found a connection between phenotype alterations of spheroids and stress-induced changes in proliferation and apoptotic rates. While in the former ones no significant changes in



(a) Percentage of actively proliferating cells grouped by spheroids diameter size. (b) Percentage of cells undergoing apoptosis grouped by spheroids diameter size.

Figure 1.4: Cellular characteristics of 28-day-old spheroids. [1]

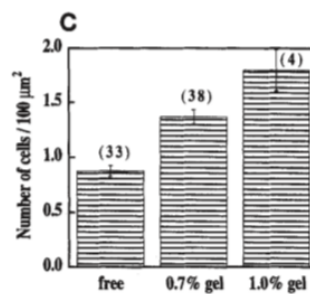


Figure 1.5: Cell density. Mean \pm SE of the spheroid population is shown. [1]

proliferative rates were detected, on the other hand, in the latter they found that cell division was higher in regions of lower stress (i.e., in the direction of the major axis of oblate spheroids) as shown in fig.(1.8).

For what concerns cell-programmed death's phenomenon, Helmlinger found a direct correlation between imposed solid stress and the decrease of apoptotic rates in the central regions of the tumour. Contrarily, Cheng et al. examined the entire area of the growing spheroids observing that an augment of external stress levels corresponds to an increase in cell death rates. Apoptosis and consequential necrosis were found either in 0.5% and 1% agarose gels. Since compressive stress is responsible for cell death, there should be similar scenarios either if the stress is growth induced or externally applied. For this reason, Cheng et al. compressed monolayers of cancer cells for 17hr with pressures which vary in a range from 0 mmHg to 60 mmHg, noting an augment in cell apoptosis rates once the stress levels had been increased. Then the growing spheroids were transferred from free suspensions into 1% agarose gel and cultured under three conditions: normal medium with and without external compression, starvation medium without external compression. Apoptosis cell death was recorded through the Caspase3 activity, since sequential activation of caspases plays a central role in the execution-phase of cell apoptosis.

Compression caused a significant increase in Caspase3 activity (as shown in fig.(1.9)): spheroids experiencing starvation showed much less apoptosis than those which were under normal nutrient conditions but stressed. The reverse attitude in apoptotic rates between unstressed spheroids and stressed indicates

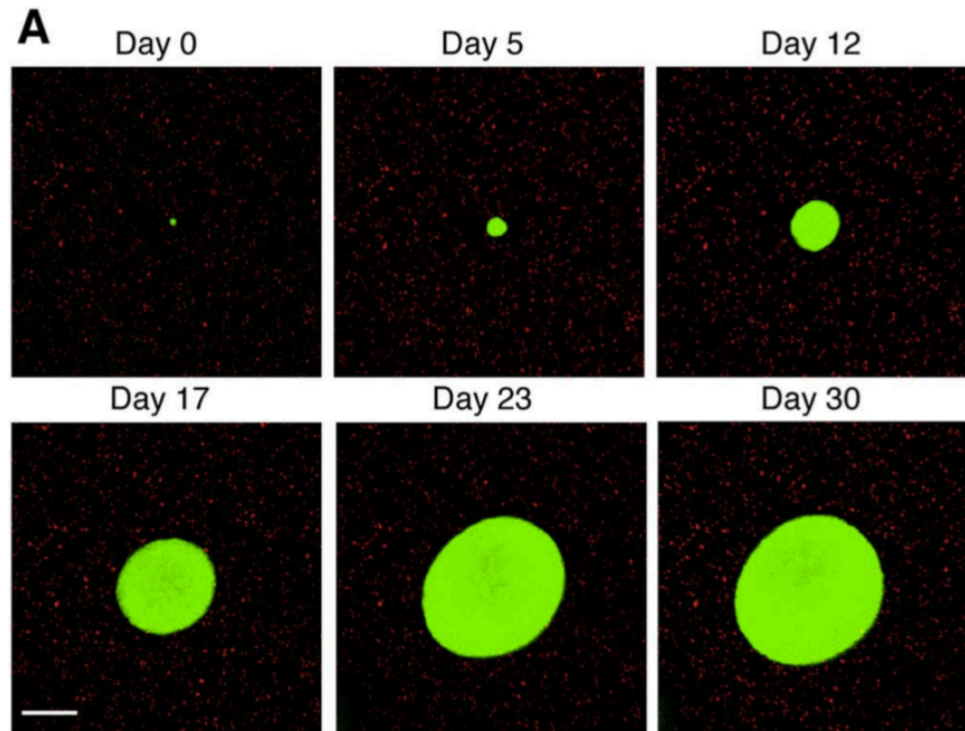


Figure 1.6: Mechanical stress accumulates around growing tumour spheroids. [5]

that nutrient starvation cannot be considered the only responsible factor in cell death.

Hence, in Helmlinger experiments, although free-suspensions spheroids were subjected to nutrient limitations, they grew faster than gel-embedded spheroids in rich-nutrient conditions.

Based on the previous discussion, we can state that the stress field imposed on a tumour by the neighboring tissue (in vivo) or an external matrix (in vitro), as well as that generated internally by cells binds during expansion, can play a pivotal role in tumour regulation. However, it has been detected experimentally that within a spheroid there are three distinct regions: an external thin layer of proliferating cells, a central region of quiescent cells, and an inner part of waste and disintegrated cell material referred to as the necrotic region. Several models exploited the concepts of oxygen diffusion, growth's and death's rate dependence on nutrient levels, porous media theory to predict migration of cells. The occurrence of necrosis is then made dependent on the attainment of a critical oxygen concentration threshold. The assumption that there is a strong correlation between necrosis and nutrient's lack has been put into question by experimental data. The experimental observations did show several behaviours in different cell types grown in spheroids: some exhibit necrotic regions closely linked to oxygen concentrations, but most do not display this attitude. Cell types, such as EMT6, may not have necrotic regions even in low levels of oxygen concentrations. For this reason, alternative biological mechanisms should be taken into account to investigate the formation and the dynamics of necrosis.

A possible approach, inspired by Helmlinger experiments, is to consider the pressure generated by the motion of the extracellular fluid and the intercellular

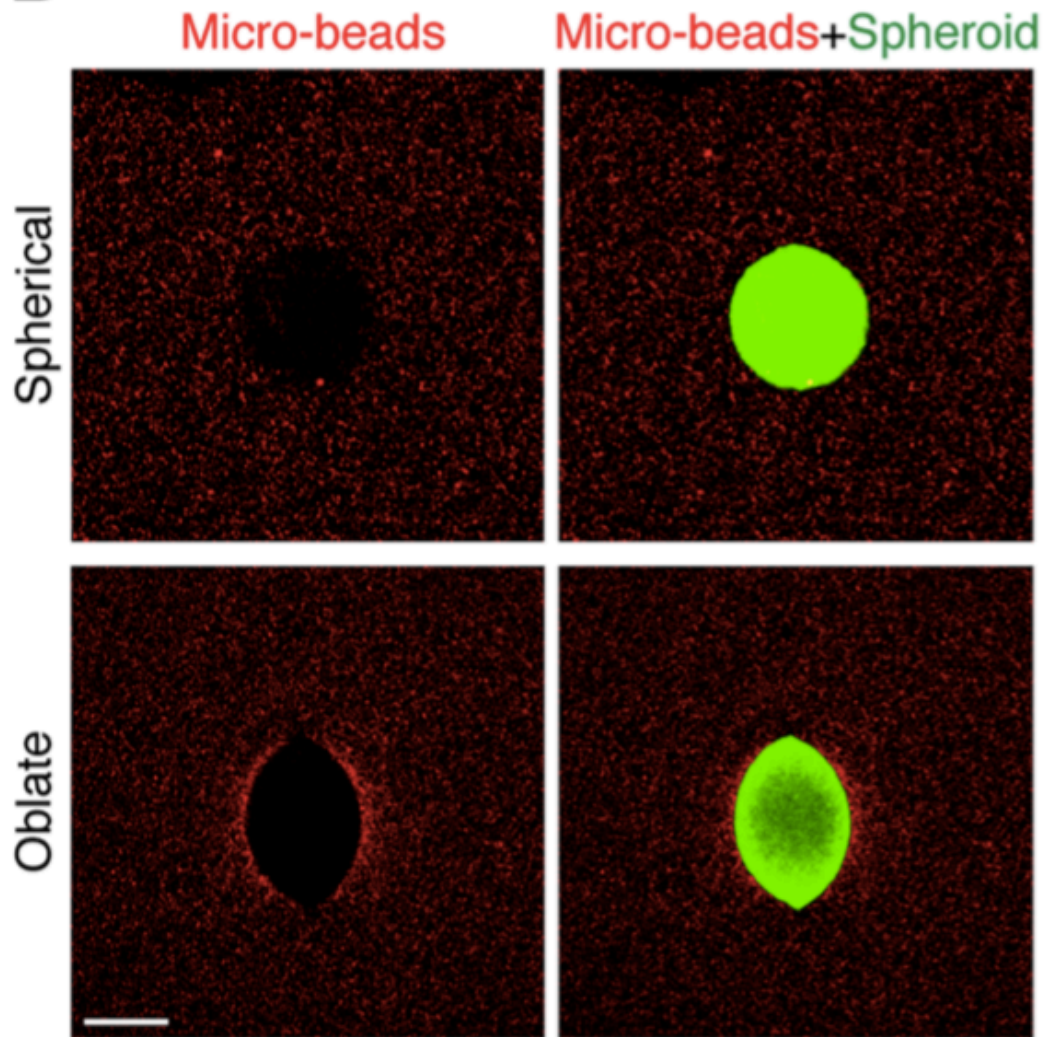


Figure 1.7: Spheroids (green) of different shapes and their surrounding stress fields visualized by micro-beads (red). [5]

pressures created by cellular migration. The existence of the necrotic region is subjected by the requirement that the nature of forces between cells must be of the compressive type, make them weakly able to give origin to tensile strengths. When these forces become weak such that fluid pressure turns to be greater than the cell pressure, necrosis shows up: cells die simultaneously releasing fluid and filling their previous space. In this way, the remaining live cells will only float in the surrounding dead cells material, no longer able to exert any strength. Hence, the tumour is then comprised of two main regions: an outermost in which cells are at their maximum packing density and reproduce, grow and die; an innermost at a lower packing density where cells float in the extracellular fluid.

A mathematical model is then adopted to adequately describe the growth of an avascular tumour spheroid in a deformable gel, with the aim of reproducing Helmlinger experiments. A particular focus is posed on how the mechanical properties of the exterior environment affect tumour growth dynamics. The tumour is treated as a two-phase material: cells and extracellular fluid where chemical compounds or extracellular nutrients are free to diffuse and navigate.

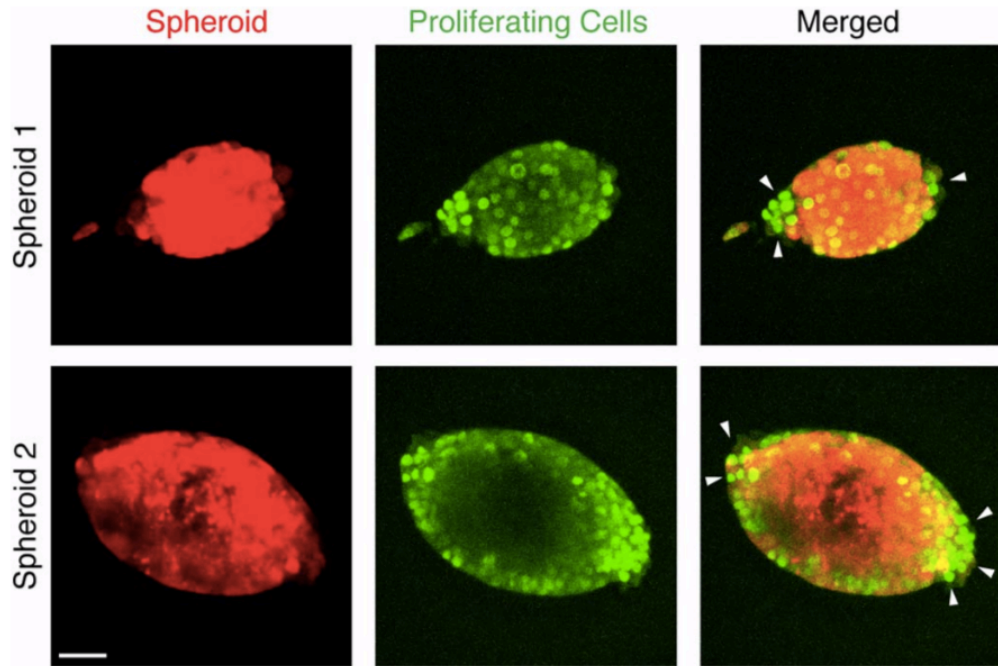


Figure 1.8: Cancer cell proliferation (green) in tumour spheroids (red) is suppressed in the direction of higher mechanical stress. *Arrowheads indicate the regions with more cell proliferation.* [5]

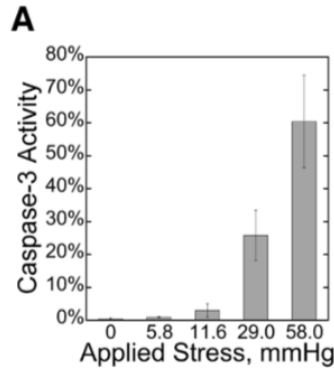
This mathematical framework, presented initially by Greenspan (1976) [14], has been further analyzed in several models. In these models cells actively reproduce and die, giving origin to internal pressures of adhesion, that can be seen as expansive forces. As a consequence, surface tension is then generated by cells in the outer boundary to keep the compactness of the tumour.

Finally, the tumour model developed by Landmann and Please (2000) has been adopted in this piece of work since their model formulation allows to readily investigate the interactions between internal and external environment, one of our main goals.

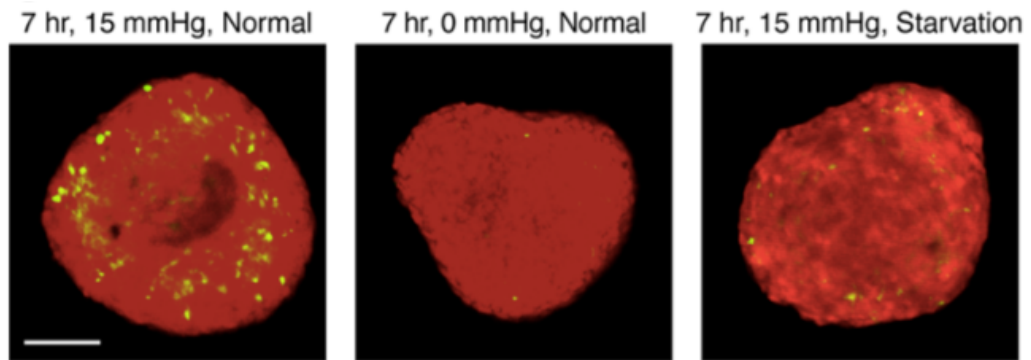
Further analysis of Landman and Please model has been carried out by Chen et al. (2001), who reproduced the same previous modelling features but changed the boundary conditions to mechanically link the tumour model with the outer tissue.

Results obtained in numerical simulations by Chen et al. [2], limitations of the model and possible modifications

The numerical simulations made by Chen et al. [2] showed a precise bifurcation in the tumour behaviour which crucially depends on the values chosen to characterize the strain energy function and consequently the Cauchy stress tensor of the external tissue. Non necrotic steady states appears for larger values of stress parameters. Also, increasing the outer tissue stiffness, it is detected that the



(a) Caspase3 activity increases in monolayers of cancer cells in response to higher external stress.



(b) Typical Caspase3 activity (green) in spheroids (red) cultured in three different conditions.

Figure 1.9: Mechanical stress-induced cell death in tumour spheroids. [5]

onset of necrosis is delayed and once necrosis is initiated the equilibrium radii of the tumour and the growth rate are reduced. Under the same displacement at the boundary, they also noted that increasing the stiffness, the growth-induced stress augments and so the cell pressures values throughout the tumour.

The numerical simulations gained by Chen et al. [2] successfully reproduced the macroscopic behaviour of the tumour, especially the growth inhibition due to the outer stress increase.

Conversely, Chen et al. [2] employed several assumptions adopted by Landman and Please in their model [6], such as the constant volume fraction and constant proliferative and death rates. Such assumptions make the tumour growth dynamics independent of the outer tissue stress until the necrosis is reached, which is not totally realistic and, for this reason, a mechano-sensitive feature would be preferred and interesting to be added.

Our attempt is to reproduce the main features of the Chen et al. [2] modelling framework, simplifying the outer tissue model: the outer tissue normal stress component which appears in the cell pressure boundary condition at the tumour radius will be treated as an elastic force acting on the tumour of varying stiffness. Such simplification has been made to investigate deeply how the onset of necrosis is retarded by the influence of the external medium's stiffness, and how the two

pressures values change by altering such force from lower values to greater ones.

This investigation has been conducted through the employment of an ODE solver on MATLAB.

Such variant to the Chen et al. model [2] has been carried out with the aim of easily changing in a further work the proliferative and death rates trying to reproduce what was recorded in Helmlinger experiments [1] for the cellular parameters.

In the following sections the Chen et al. model [2] will be interpreted through multiphase models general theory and then presented to properly comment and analyze some results and simulations gained making some simplifications and alteration to the Chen modelling framework.

Chapter 2

Multiphase Models

2.1 Mass and momentum balances

Mixture theory has been exploited through the years for the description of the mechanics of biological tissues with a particular focus on the behaviour of articular cartilages, soft tissues, heart mechanics, subcutaneous layer, flow through arteries [3]. During last decades it has been successfully applied also to tumour growth. In general soft tissues are mostly composed of cells and extracellular matrix. Their structure can be associated with a porous material wet by an extracellular liquid rich of chemical compounds. Here, the growth of the tumour is modelled through porous media theory combining mass and force balances for each phase including the concepts of diffusion-limited growth response to an external nutrient.

For each phase, it is possible to define the volume ratio as follows. Given a fixed point in the mixture, let it be the center of a sequence of different sample volumes. As it can be seen in fig. (2.1), for sizes smaller than a cell we are not able to measure the ratio of the volume of a given constituent inside the sample to the volume of the sample volume in a stable way because of the evident fluctuations caused by the microscopic inhomogeneities. A similar scenario is gained at the tissue scale, where strong macroscopic inhomogeneities might occur making it impossible to define properly the volume ratio. For intermediate scales included in a spatial range greater than cellular sizes and smaller than tissue levels, it is feasible to characterize the volume fraction as a function of sample volume size (fig. (2.1)).

For such scales, regarding the tumour as a two-phase mixture (tumour cells and extracellular fluid), we can associate with tumour cells and the external fluid the volume fractions ϕ_c and ϕ_e and the densities ρ_c and ρ_e respectively.

Mass balances applied to each phase are:

$$\begin{aligned}\frac{\partial \phi_c \rho_c}{\partial t} + \nabla \cdot (\rho_c \phi_c \mathbf{U}_c) &= \Gamma_c \\ \frac{\partial \rho_e \phi_e}{\partial t} + \nabla \cdot (\rho_e \phi_e \mathbf{U}_e) &= \Gamma_e,\end{aligned}\tag{2.1}$$

with Γ_c and Γ_e being phases mass source terms and \mathbf{U}_c and \mathbf{U}_e cell and fluid velocities.

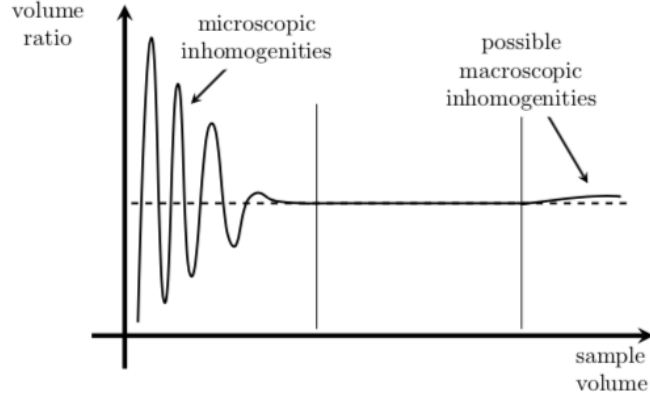


Figure 2.1: Volume fraction of the constituent as a function of the volume sample size. [3]

If we sum both the equations in (2.1):

$$\begin{aligned}
 \frac{\partial}{\partial t} \underbrace{(\rho_c \phi_c + \rho_e \phi_e)}_{\substack{\rho_m \\ \downarrow \\ \text{density of the mixture}}} + \nabla \cdot \underbrace{(\rho_c \phi_c \mathbf{U}_c + \rho_e \phi_e \mathbf{U}_e)}_{\substack{\rho_m \mathbf{U}_m \\ \downarrow \\ \text{velocity of the mixture}}} &= \Gamma_c + \Gamma_e \\
 \Downarrow & \\
 \frac{\partial \rho_m}{\partial t} + \nabla \cdot (\rho_m \mathbf{U}_m) &= \Gamma_c + \Gamma_e.
 \end{aligned} \tag{2.2}$$

If we postulate that the mixture is *closed*, it holds:

$$\Gamma_c + \Gamma_e = 0 \quad \Rightarrow \quad \Gamma_e = -\Gamma_c. \tag{2.3}$$

Moreover, we define:

$$\Gamma_c = \rho_c \phi_c S(C), \tag{2.4}$$

with $S(C)$ being the net proliferation and death rate of the mixture (dependent on the local oxygen concentration) which will be characterised later in Chen et al. [2] model description.

If we assume the incompressibility of the material constituting each phase, then ρ_c and ρ_e are constants that can be simplified in the above equations (2.1). In addition, we assume that $\rho_c = \rho_e = \rho$; that, recalling the definition for the cell mass source term (2.4), allows to write the mass balance equations as:

$$\begin{aligned}
 \frac{\partial \phi_c}{\partial t} + \nabla \cdot (\phi_c \mathbf{U}_c) &= \phi_c S(C) \\
 \frac{\partial \phi_e}{\partial t} + \nabla \cdot (\phi_e \mathbf{U}_e) &= -\phi_c S(C).
 \end{aligned} \tag{2.5}$$

For what concerns the momentum balances, inertial forces can be neglected, thus leading to [13]:

$$\begin{aligned}\nabla \cdot \mathbb{T}_c + \mathbf{m}_c &= \mathbf{0} \\ \nabla \cdot \mathbb{T}_e + \mathbf{m}_e &= \mathbf{0},\end{aligned}\tag{2.6}$$

where \mathbf{m}_c and \mathbf{m}_e represent a momentum exchange term due to the interactions of the phases and \mathbb{T}_c and \mathbb{T}_e are the phase stress tensors.

If we postulate the momentum conservation of the mixture, defining its stress tensor as $\mathbb{T}_m = \mathbb{T}_c + \mathbb{T}_e$, it holds:

$$\nabla \cdot \mathbb{T}_m = \nabla \cdot (\mathbb{T}_c + \mathbb{T}_e) = \mathbf{0}.\tag{2.7}$$

Equations (2.6) and (2.7) are compatible if:

$$\sum_{\alpha=c,e} \mathbf{m}_\alpha = \mathbf{0}.\tag{2.8}$$

2.2 Characterization of Phases Stress Tensors

2.2.1 Saturation Hypothesis

If we assume that the mixture is saturated, it means:

$$\phi_c + \phi_e = 1.\tag{2.9}$$

Under such an assumption, the mass balances (2.1) with the hypothesis of closed mixture (2.3) and constant and equal densities for both phases ($\rho = \rho_c = \rho_e$), if summed together, give:

$$\begin{aligned}\nabla \cdot (\phi_c \mathbf{U}_c + \phi_e \mathbf{U}_e) &= 0 \\ \Downarrow \\ \phi_c \nabla \cdot \mathbf{U}_c + \phi_e \nabla \cdot \mathbf{U}_e + \mathbf{U}_c \cdot \nabla \phi_c + \mathbf{U}_e \cdot \nabla \phi_e &= 0 \\ \Downarrow \\ \phi_c \operatorname{tr} \mathbb{L}_c + \phi_e \operatorname{tr} \mathbb{L}_e - (\mathbf{U}_c - \mathbf{U}_e) \cdot \nabla \phi_e &= 0,\end{aligned}\tag{2.10}$$

with \mathbb{L}_α ($\alpha = c, e$) being the velocity gradient related to each phase. The last two lines of (2.10) can be considered the kinematic version of the saturation constraint. Such a kinematic constraint leads to indeterminacy in the phases stress tensors and the momentum exchange terms, which corresponds to solve a constrained problem which acquires a specific form through the second law of thermodynamics.

To achieve the final form of the constrained problem, we have firstly to introduce the Clausius-Duhem inequality for a multiphase mixture.

To this end, we can write the energy equation for both the phases of the mixture (under the above hypothesis of constant and equal density ρ for both phases):

$$\begin{aligned}\rho \left[\frac{\partial \phi_\alpha \varepsilon_\alpha}{\partial t} + \nabla \cdot (\phi_\alpha \varepsilon_\alpha \mathbf{U}_\alpha) \right] &= \operatorname{tr} (\mathbb{T}_\alpha \mathbb{L}_\alpha) - \nabla \cdot \mathbf{q}_\alpha + \rho \phi_\alpha r_\alpha + e_\alpha \\ \alpha &= c, e;\end{aligned}\tag{2.11}$$

where:

- ε_α is the specific internal energy;
- \mathbf{q}_α is the partial heat supply density;
- r_α is the heat supply density;
- e_α is the energy supply related to energy exchange between the phases;
- $\mathbb{L}_\alpha = \nabla \mathbf{U}_\alpha$ is the velocity gradient.

Before approaching the second principle of thermodynamics, it is necessary to give the following definitions:

- $(\dot{\cdot}) = \frac{\partial(\cdot)}{\partial t} + \mathbf{U}_m \cdot \nabla(\cdot)$ with $\mathbf{U}_m = \sum_{\alpha=c,e} \frac{\rho\phi_\alpha \mathbf{U}_\alpha}{\rho_m}$ the velocity of the mixture already encountered in (2.2),
- the total heat supply density $r_m = \frac{1}{\rho_m} \sum_{\alpha=c,e} \rho\phi_\alpha r_\alpha$,
- $\mathbf{w}_\alpha = \mathbf{U}_\alpha - \mathbf{U}_m$ the diffusion velocity related to each phase.

If we consider that each phase has the same temperature θ and that the second law of thermodynamics holds true for the mixture as a whole, the Clausius-Duhem inequality can be written ([13]):

$$\rho_m \dot{\eta}_m + \nabla \cdot \left(\sum_{\alpha=c,e} \frac{\mathbf{q}_\alpha + \rho\phi_\alpha \eta_\alpha \theta \mathbf{w}_\alpha}{\theta} \right) - \sum_{\alpha=c,e} \frac{\rho\phi_\alpha r_\alpha}{\theta} \geq 0, \quad (2.12)$$

where η_α is the specific entropy of the α -phase and $\eta_m = \sum_{\alpha=c,e} \frac{\rho\phi_\alpha \eta_\alpha}{\rho_m}$ is the entropy density for the whole mixture.

Defining $\mathbf{h} = \sum_{\alpha=c,e} (\mathbf{q}_\alpha + \rho\phi_\alpha \eta_\alpha \theta \mathbf{w}_\alpha)$ the entropy flux for the mixture as a whole [13] and recalling the definition for r_m previously given, we can write (2.12) in a more compact form as follows:

$$\rho_m \dot{\eta}_m + \nabla \cdot \left(\frac{\mathbf{h}}{\theta} \right) - \frac{\rho_m r_m}{\theta} \geq 0, \quad (2.13)$$

It is useful to write the previous formulation (2.12) of the second law of thermodynamics in a way such that constitutive relations for momentum exchange terms can be outlined.

With this purpose we write the energy equation for the whole mixture:

$$\rho_m \dot{\varepsilon}_\alpha^I = tr \left(\sum_{\alpha=c,e} \mathbb{T}_\alpha \mathbb{L}_\alpha \right) - \nabla \cdot \mathbf{q}_m^I - \sum_{\alpha=c,e} \mathbf{U}_\alpha \cdot \mathbf{m}_\alpha + \rho_m r_m, \quad (2.14)$$

where [13]:

- $\varepsilon_m^I = \sum_{\alpha=c,e} \left(\frac{\rho\phi_\alpha\varepsilon_\alpha}{\rho_m} \right)$, the so called inner part of the internal energy for the mixture;
- $\mathbf{q}_m^I = \sum_{\alpha=c,e} (\mathbf{q}_\alpha + \rho\phi_\alpha\varepsilon_\alpha\mathbf{w}_\alpha)$, that can be considered the heat flux for the mixture.

We can now introduce the following quantities [13]:

- $\psi_\alpha = \varepsilon_\alpha - \theta\eta_\alpha$, the specific Helmotz free energy for the α -phase;
- $\mathbb{H}_\alpha = \psi_\alpha\mathbb{I} - \frac{1}{\rho_\alpha\phi_\alpha}\mathbb{T}_\alpha$, the chemical potential tensor for the α -phase;
- $\Psi_\alpha = \rho\phi_\alpha\psi_\alpha$, Helmotz free energy related to the α -phase.

Exploiting (2.14), and the definition given above for the \mathbf{q}_m^I the heat flux of the mixture, it is feasible to write the subsequent reformulation of the second law of thermodynamics (2.13):

$$-\rho_m\eta_m\dot{\theta} - \sum_{\alpha=c,e} \Psi'_\alpha \geq \text{tr} \left(\sum_{\alpha=c,e} \rho\phi_\alpha\mathbb{H}_\alpha\mathbb{L}_\alpha \right) + \mathbf{h} \cdot \frac{\nabla\theta}{\theta} + \sum_{\alpha=c,e} \mathbf{m}_\alpha \cdot \mathbf{U}_\alpha, \quad (2.15)$$

where

$$(\cdot)' = \frac{\partial(\cdot)}{\partial t} + \mathbf{U}_\alpha \cdot \nabla(\cdot). \quad (2.16)$$

Thus, the final version of the constrained problem, presented at the beginning of the section, under the saturation hypothesis, can be written as:

$$-\rho_m\eta_m\dot{\theta} - \sum_{\alpha=c,e} \Psi'_\alpha - \mathbf{h} \cdot \frac{\nabla\theta}{\theta} \geq \text{tr} \left[\sum_{\alpha=c,e} \phi_\alpha (\rho\mathbb{H}_\alpha - \lambda\mathbb{I}) \mathbb{L}_\alpha \right] + (\mathbf{m}_e - \lambda\nabla\phi_e) \cdot (\mathbf{U}_e - \mathbf{U}_c), \quad (2.17)$$

for any scalar multiplier λ .

The preceding inequality (2.17) has to hold true for every temperature (θ) distribution and stress configuration. We can put in a stress-free configuration, isothermal case, and analyse:

$$(\mathbf{m}_e - \lambda\nabla\phi_e) \cdot (\mathbf{U}_e - \mathbf{U}_c) \leq 0, \quad (2.18)$$

which suggests the following constitutive relation for \mathbf{m}_e :

$$(\mathbf{m}_e - \lambda\nabla\phi_e) = -\alpha(\mathbf{U}_e - \mathbf{U}_c), \quad (2.19)$$

such that the inequality (2.18) is satisfied, being α a scalar parameter. In fact, if (2.19) holds true, (2.18) becomes:

$$-\alpha|\mathbf{U}_e - \mathbf{U}_c|^2 \leq 0, \quad (2.20)$$

which is obviously respected.

Thus, the two stress tensors acquire the following mathematical structure:

$$\begin{aligned}\mathbb{T}_c &= -\phi_c P_e \mathbb{I} + \mathbb{T}'_c \\ \mathbb{T}_e &= -\phi_e P_e \mathbb{I} + \mathbb{T}'_e,\end{aligned}\tag{2.21}$$

with P_e representing the extracellular fluid pressure, \mathbb{T}'_c and \mathbb{T}'_e being the phases stress tensors' parts related to the constitutive laws chosen to describe how the particular material replies mechanically to a specific strain following a determined motion.

For what regards the momentum exchange terms, under the momentum conservation (2.8), we have:

$$\mathbf{m}_c = -\mathbf{m}_e.\tag{2.22}$$

Thus, we can focus on the analysis of the \mathbf{m}_e term. Through (2.19), its structure can be split in two different contributions:

$$\mathbf{m}_e = P_e \nabla \phi_e + \mathbf{m}'_e,\tag{2.23}$$

where λ has been substituted with P_e , and $\mathbf{m}'_e = -\alpha (\mathbf{U}_e - \mathbf{U}_c)$.

The first term on the right-hand side of the equality accounts for distribution of the stress within the material also in equilibrium circumstances due not to dissipation, differently from the second one (\mathbf{m}'_e) which describes what kind of dissipation forces arises as a consequence of a particular motion.

The aforesaid separation in two different contributions in the momentum equation of the exchange term derives from the analysis conducted before, but alternatively it can be achieved also by a profound study of the dissipation function, which has to fulfill the second thermodynamic principle [11].

2.2.2 Constant Cell Volume Fraction

It is found in experiments that the volume ratio of multicellular spheroids grown in vitro does not change much. So, the first models dealing with tumour growth, starting from Greenspan [14], started from the assumption that it can be taken constant (or nearly constant). Treating the cell volume fraction as a scalar constant implies the addition of another mechanical constraint that both the phases need to satisfy, thus giving rise to one more Lagrangian multiplier.

We can prove it by doing the same analysis conducted before.

Through the saturation (2.9), if the cell volume fraction is constant, we are allowed to write:

$$\Rightarrow \left. \begin{aligned} \phi_c &= const. \\ \phi_e &= 1 - \phi_c = const. \end{aligned} \right\} \Rightarrow \left. \begin{aligned} \phi_c &= \bar{\phi} = const. \\ \phi_e &= \tilde{\phi} = const. \end{aligned} \right\} \tag{2.24}$$

Hence, for each phase, we have that the mass balances can be rewritten:

$$\begin{aligned}\phi_c \operatorname{tr}(\mathbb{L}_c) &= \frac{\Gamma_c}{\rho} \\ \phi_e \operatorname{tr}(\mathbb{L}_e) &= \frac{\Gamma_e}{\rho}\end{aligned}\tag{2.25}$$

We have thus achieved the kinematic constraint derived from the constant cell volume fraction assumption: as in the saturation hypothesis, also here we an indeterminacy reflected in phases stress tensors and momentum exchange terms, which can be solved again as a constrained problem considering the following formulation of the second law of thermodynamics:

$$\begin{aligned}-\rho_m \eta_m \dot{\theta} - \sum_{\alpha=c,e} \Psi'_\alpha - \mathbf{h} \cdot \frac{\nabla \theta}{\theta} \geq \operatorname{tr} \left[\sum_{\alpha=c,e} \phi_\alpha (\rho \mathbb{H}_\alpha) \right] - \phi_c \bar{\lambda} \operatorname{tr}(\mathbb{L}_c) - \phi_e \tilde{\lambda} \operatorname{tr}(\mathbb{L}_e) \\ + \left(\mathbf{m}_e - \bar{\lambda} \frac{\Gamma_c}{\rho} - \tilde{\lambda} \frac{\Gamma_e}{\rho} \right) \cdot (\mathbf{U}_e - \mathbf{U}_c),\end{aligned}\tag{2.26}$$

for any couple of scalar multipliers $\bar{\lambda}$ and $\tilde{\lambda}$.

Such a constrained problem gives rise to the following phases stress tensors structures:

$$\begin{aligned}\mathbb{T}_c &= -\bar{\lambda} \mathbb{I} + \mathbb{T}'_c \\ \mathbb{T}_e &= -\tilde{\lambda} \mathbb{I} + \mathbb{T}'_e\end{aligned}\tag{2.27}$$

The assumption of constant volume ratio leads also to a different structure of the momentum exchange terms compared to (2.23):

$$\mathbf{m}_e = -\alpha (\mathbf{U}_e - \mathbf{U}_c).\tag{2.28}$$

2.3 Momentum Balances Reformulation

Neglecting shear stresses, gravitational influences, inertial forces momentum balances become force balances. In particular, Chen et al. [2] considered that the forces acting on a point of the mixture are: the hydrodynamic drag force, hydrostatic force and intercellular force.

Denoting by P_c and P_e the cell and the fluid pressure, the force balance for tumour cells is:

$$-\frac{1}{\kappa} \phi_c (\mathbf{U}_c - \mathbf{U}_e) - \phi_c \nabla P_e - \nabla P_c = \mathbf{0},\tag{2.29}$$

where κ is the constant of permeability, representing the ease with which extracellular fluid travels through the extracellular matrix. As we can see in (2.29), the drag force and the hydrostatic pressure gradient exerted by a cell volume fraction ϕ_c must be counterbalanced by the intercellular pressure gradient.

For the extracellular fluid the hydrodynamic drag force and the hydrostatic pressure exerted by cells must balance the hydrostatic fluid pressure, thus leading to:

$$\frac{1}{\kappa}\phi_c(\mathbf{U}_c - \mathbf{U}_e) + \phi_c\nabla P_e - \nabla P_e = \mathbf{0}. \quad (2.30)$$

We can now compare the momentum balances equations (2.6) written in (2.1) with (2.29) and (2.30), characterising the constants $\bar{\lambda}$ and $\tilde{\lambda}$ encountered in (2.27).

Firstly, we can analyse the fluid phase momentum balance equation:

$$\nabla \cdot \mathbb{T}_e + \mathbf{m}_e = \mathbf{0}. \quad (2.31)$$

Recalling the stress tensors structures in (2.27) and neglecting shear stresses in the fluid phase (i.e., neglecting \mathbb{T}'_e) and exploiting the characterisation of the fluid momentum exchange term \mathbf{m}_e in (2.28), equation (2.31) can be written as:

$$-\nabla \tilde{\lambda} + \alpha(\mathbf{U}_c - \mathbf{U}_e) = \mathbf{0}. \quad (2.32)$$

Comparing (2.32) with (2.30), we can set:

- $\tilde{\lambda} = (1 - \phi_c)P_e = \phi_e P_e;$
- $\alpha = \phi_c \frac{1}{\kappa}.$

Thus, we have found the connection of stress tensors' structure in (2.21) with the one in (2.27), having fully characterised $\tilde{\lambda}$.

Focusing now on the tumour cells momentum balance:

$$\nabla \cdot \mathbb{T}_c + \mathbf{m}_c = \mathbf{0}, \quad (2.33)$$

we can repeat the same analysis conducted before for the fluid phase. Neglecting shear stresses in (2.27) and remembering the momentum conservation introduced in (2.8) that allows to characterise the \mathbf{m}_c term through (2.28), equation (2.33) can be rewritten as:

$$-\nabla \bar{\lambda} + \alpha(\mathbf{U}_e - \mathbf{U}_c) = \mathbf{0}. \quad (2.34)$$

Comparing (2.34) with (2.29):

- $\bar{\lambda} = \phi_c P_e + P_c;$
- $\alpha = \phi_c \frac{1}{\kappa}.$

As we can see, there is a clear difference between the characterisation given in (2.21) and the one in (2.27) in the tumour cells stress tensor: in this case, the appearance of another Lagrangian multiplier (P_c) accounts for the constant cells volume fraction constraint.

2.4 The surrounding medium

Characterization of the strain energy function [12]

In case of isotropy, if a material is *incompressible*, then the strain energy function can be written as:

$$W(\mathbb{B}) \equiv \hat{W}(\bar{I}_1, \bar{I}_2, \bar{I}_3) = \hat{\mathcal{V}}(\bar{I}_1, \bar{I}_2) + \hat{\mathcal{U}}(\bar{I}_3) \quad (2.35)$$

with $\hat{\mathcal{U}}$ being an affine function of \bar{I}_3 , such as $\hat{\mathcal{U}}(\bar{I}_3) = \theta(\bar{I}_3 - 1)$ (being θ an arbitrary scalar constant).

If the material is *quasi-incompressible* (alternatively *weakly compressible*), then the strain energy function can be decomposed as the incompressible case in two different contributions:

$$W(\mathbb{B}) \equiv \hat{W}(\bar{I}_1, \bar{I}_2, \bar{I}_3) = \mathcal{V}(\bar{I}_1, \bar{I}_2) + \mathcal{U}(\bar{I}_3) \quad (2.36)$$

but with \mathcal{U} not necessarily being an affine function of \bar{I}_3 . For example, in the case of the Chen et al. [2] model, $\mathcal{U}(\bar{I}) = \gamma \frac{(\bar{I}_3 - 1)^2}{(\bar{I}_3 - \delta)^n}$.

The stress coming from $\hat{\mathcal{V}}$ is **always**-by definition- deviatoric, whilst the stress coming from $\hat{\mathcal{U}}$ takes into account the volumetric deformations.

Chen et al. [2] strain energy function

As already stated, Chen et al. [2] assumed that the tumour aggregate is embedded in an isotropic elastic tissue characterized through a hyperelastic strain density function suggested by Helmlinger [1]:

$$W = \eta \left(e^{\beta(\bar{I}_1 - 3)} - \bar{I}_1 \right) + \gamma \frac{(\bar{I}_3 - 1)}{(\bar{I}_3 - \delta)^n}, \quad (2.37)$$

where the empirically determined parameters η, β, γ and n are positive and δ stands for the solid fraction of the medium.

The usual strain invariants of an isotropic pure elastic solid I_1, I_2 and I_3 have been redefined in the following way:

$$\begin{aligned} \bar{I}_1 &= I_3^{-\frac{1}{3}} I_1 \\ \bar{I}_2 &= I_3^{-\frac{2}{3}} I_2 \\ \bar{I}_3 &= I_3 \end{aligned} \quad (2.38)$$

The usual strain invariants are given, instead, by:

$$\begin{aligned} I_1 &= \text{tr} \mathbb{B} \\ I_2 &= \frac{1}{2} \{ (\text{tr} \mathbb{B})^2 - \text{tr}(\mathbb{B}^2) \} \\ I_3 &= \det \mathbb{B}, \end{aligned} \quad (2.39)$$

where \mathbb{B} is the *left Cauchy-Green deformation tensor* $\mathbb{F} \cdot \mathbb{F}^T$, with \mathbb{F} being the deformation gradient tensor.

The energy function Chen et al. [2] decided to employ is a little modification of (2.37) and satisfies the condition of no stress at no displacement:

$$W = \eta \left(e^{\beta(\bar{I}_1 - 3)} - 1 \right) + \gamma \frac{(\bar{I}_3 - 1)^2}{(\bar{I}_3 - \delta)^n}. \quad (2.40)$$

Physical Meaning of the Empirical Parameters in the Strain Energy Function

Developing (2.40) respect to small deformations and keeping only the quadratic terms and finally making the comparison with the linear elasticity case, we gain:

$$\begin{aligned} \mu &= 2\eta\beta \\ \lambda &= \frac{8\gamma}{(1-\delta)^n} - \frac{4}{3}\eta\beta, \end{aligned} \quad (2.41)$$

where μ and λ are the Lamé constants (provided $\lambda > 0$ is satisfied), which are related to the bulk modulus:

$$\kappa = \lambda + \frac{2}{3}\mu. \quad (2.42)$$

Thus, exploiting (2.41), we can infer that:

$$\kappa = \frac{8\gamma}{(1-\delta)^n}. \quad (2.43)$$

As we can see in the previous relations γ , δ and n of the strain energy function appear in the definition of the bulk modulus κ , instead η and β are related to the shear modulus μ .

Equations of motion for the tissue model

Neglecting the fluid pore pressure in the surrounding medium, the constitutive equation adopted to model the tissue is typical for non-linear elastic solids; in fact, the Cauchy stress tensor has the following shape:

$$\mathbb{T} = 2(I_3)^{-\frac{1}{2}} \{J_3 W_3 \mathbb{I} + W_1 \mathbb{B}\}, \quad (2.44)$$

where I_3 is the usual strain invariant introduced before, and for the sake of brevity the following notations have been adopted in the constitutive law of the tissue in (2.44):

$$\begin{aligned} W_1 &= \frac{\partial W}{\partial I_1}, \\ W_3 &= \frac{\partial W}{\partial I_3}. \end{aligned} \quad (2.45)$$

As usual, neglecting inertia contributes, the equations of motion for the tissue are:

$$\nabla \cdot \mathbb{T} = \mathbf{0}. \quad (2.46)$$

As for the tumour model, a non-dimensionalisation of the tissue model has been made and the overbars on the rescaled variables have been omitted. Radial symmetry is employed also for the surrounding medium and Chen et al. [2] assume that growth occurs in the radial direction and such a postulation leads to a simple structure of the representation of the stress tensor in polar coordinates, with a lot of components being null: the only non-vanishing components remain σ_{rr} , $\sigma_{\theta\theta}$ and $\sigma_{\phi\phi}$.

Though the equilibrium equations are:

$$\begin{aligned} \frac{\partial \sigma_{rr}}{\partial r} + \frac{2}{r} (\sigma_{rr} - \sigma_{\theta\theta}) &= 0 \\ \sigma_{\theta\theta} &= \sigma_{\phi\phi}. \end{aligned} \quad (2.47)$$

We can now reformulate the previous equations (2.47) by introducing the definition of displacement $u = r - R$, where r and R are the radial spatial and material coordinates respectively.

Through such definition, equations of motion (2.47) can be reduced to:

$$f \left(R, u, \frac{\partial u}{\partial R} \right) \frac{\partial^2 u}{\partial R^2} - g \left(R, u, \frac{\partial u}{\partial R} \right) \left(\frac{\partial u}{\partial R} - \frac{u}{R} \right) = 0, \quad (2.48)$$

where $f \left(R, u, \frac{\partial u}{\partial R} \right)$ and $g \left(R, u, \frac{\partial u}{\partial R} \right)$ are functions defined in Appendix A of the Chen et al. [2] paper.

Equation (2.48) is subjected to the following boundary conditions:

$$\begin{aligned} u &= X(t) - X_0 \text{ at } R = X_0, \\ u &\rightarrow 0 \text{ as } R \rightarrow \infty, \end{aligned} \quad (2.49)$$

where X_0 is the initial radius of the tumour and $X(t)$ is the radius at time t .

Chapter 3

Mathematical Model

3.1 Physical description of Chen et al. Model [2]

In the initial stage, the tumour is assumed to be sufficiently small to consider a plentiful supply of oxygen, which enables cells to reproduce driving expansion readily. As the non-necrotic spheroid carries on expanding, the oxygen levels start to decay, and cells begin to die of nutrient starvation.

One of the primary assumptions of Chen et al. [2] model is the constant volume fraction: to maintain the compactness of the region, while cells are dying, the remaining living cells will either move outwards to ensure expansion inwards to push out the liquid released by the dead cells. In the region where the cells die (of apoptosis), there will be an accumulation of extracellular fluid leading to an increase of fluid pressure and a sequential decrease of the cellular-bonds of adhesion. Thus, it is assumed in [2] that if, the fluid pressure equals the cell pressure, the region ceases to be compact and, thus, necrosis is initiated.

3.2 Introduction to the model

The tumour model is basically a two-phase model: one is constituted by the ensemble of extracellular membrane which keeps together the cells structure; the other is the extracellular fluid in which nutrients and chemical compounds are free to navigate, considered as an ideal fluid.

A quasi-steady reaction diffusion equation is adopted for local oxygen concentration which flows in the extracellular fluid; such equation is then combined with mass balances applied to each phase, given the dependence of net growth and death rate on the local oxygen concentration.

In Chen et al. [2] model, inertia forces are neglected, gaining a force balance for unit volume applied to each phase. In fact, they consider that, a balance between the hydrodynamic drag force, the interstitial fluid pressure and cell pressure (the so-called expansive forces) must hold, as it can be seen in (2.29) and (2.30). Then, summing together the force balances and postulating radial symmetry (given the spheroid structure of the tumour under exam), they obtain a constraint on both the pressures, that will be better specified with the introduction of the boundary condition. Such constraint is pivotal for the onset of necrosis, which crucially depends on the outer tissue stiffness through the boundary condition imposed on

the cell pressure at the outer radius. In fact, this link establishes that the pressures are equal and opposites and differ from a vertical translation at each space point which varies with time and is regulated by the outer tissue's normal stress tensor component evaluated at the tumour radius. Depending on the outer tissue constitutive law, different scenarios can take place. To reproduce Helmlinger experiments [1], Chen et al. [2] theorised that the tumour is implanted in an isotropic (porous) elastic medium, which is constitutively characterized through a hyperelastic strain energy function suggested by Helmlinger [1]. Exploiting this density strain energy function (which describes the properties of a compressible material) and neglecting the fluid pore pressure, the constitutive law chosen to describe the surrounding medium is the one typical of a non-linear elastic solid. Also in the external model inertial forces in the momentum balance equations are neglected. Under radial symmetry hypothesis, equilibrium equations are thus written for the tissue as well, and its model is coupled with the tumour model via the boundary condition posed on the cell pressure at the tumour radius.

Such a modelization of the outer tissue has the intent of recreating the stresses generated in the external environment by the progressive displacement of the tumour aggregate in the tissue: in fact, while expanding, the mass pushes against the host tissue, which in turn, depending on its mechanical properties, replies to the physical stimuli received. Moreover, the higher is the induced-stress, the more the external medium is able to compress the tumour and push out the liquid released by the dying cells, giving rise to non-necrotic steady states.

According to the physical description of the tumour model, necrosis has a great relevance and is treated differently from the previous stages of growth. One of the major novelties is to choose a mechanical occurrence of necrosis, not related to the lack of nutrient, given the remarkable role played by the external stress as observed in Helmlinger [1] and Cheng [5] experiments. The set of equations needed to describe tumour growth acquires a different structure once necrosis is initiated due to the different hypotheses that have been made during the distinct phases of expansion. Following the physical description of the model, during the initial stages of growth (nutrient rich phase and apoptosis) the spheroid grows with the constraint of keeping the same volume fraction to maintain the compactness of the region; as the apoptosis goes on, depending on the outer tissue stress shape, the fluid pressure increases until it might become equal to the cell pressure in the middle of the spheroid. In such a case the necrosis interface arises and moves with time from the center of the tumour: the region within this interface ceases to be compact and the assumption of constant cells volume fraction terminates to hold.

3.3 Chen et al. [2] model

The model In the compacted region, indicating with ϕ the cell volume ratio, and referring to section (2.1), we recall the set of equations that regulate tumour growth:

$$\begin{aligned}
\frac{\partial \phi}{\partial t} + \nabla \cdot (\phi \mathbf{U}_c) &= \phi S(C) \\
\frac{\partial(1-\phi)}{\partial t} + \nabla \cdot ((1-\phi) \mathbf{U}_e) &= -\phi S(C) \\
-\frac{1}{\kappa} \phi (\mathbf{U}_c - \mathbf{U}_e) - \phi \nabla P_e - \nabla P_c &= \mathbf{0} \\
\frac{1}{\kappa} \phi (\mathbf{U}_c - \mathbf{U}_e) + \phi \nabla P_e - \nabla P_e &= \mathbf{0}.
\end{aligned} \tag{3.1}$$

These equations are coupled with the reaction diffusion equation for the local concentration of oxygen (the only nutrient considered here) through the dependence of the net growth and death rate $S(C)$ on oxygen levels. Assuming that oxygen diffuses rapidly enough to consider a quasi-steady local concentration, we have:

$$D \nabla^2 C = \phi \Sigma(C), \tag{3.2}$$

where D is the diffusion coefficient and Σ is the oxygen consumption rate, which will be specified later.

Summing the mass balances, one gets (see also eq. (2.10)):

$$\nabla \cdot (\phi \mathbf{U}_c + (1-\phi) \mathbf{U}_e) = \mathbf{0}, \tag{3.3}$$

which, in spherical coordinates, under radial symmetry, (3.3) can be rewritten as:

$$\frac{1}{r^2} \frac{\partial}{\partial r} (r^2 \phi U_c + r^2 (1-\phi) U_e) = 0 \Rightarrow r^2 \phi U_c + r^2 (1-\phi) U_e = C(t), \tag{3.4}$$

being $C(t)$ constant in space, due to the boundary conditions imposed on the velocity field at $r = 0$.

It naturally follows that:

$$\phi U_c = -(1-\phi) U_e. \tag{3.5}$$

Instead, if we sum the force balances:

$$\nabla (P_c + P_e) = 0, \tag{3.6}$$

that, in radial symmetry, in spherical coordinates, becomes:

$$\frac{\partial}{\partial r} (P_c + P_e) = 0 \Rightarrow P_c + P_e = p(t). \tag{3.7}$$

To summarize, it holds:

$$\phi U_c = -(1-\phi) U_e, \tag{3.8}$$

$$P_c = -P_e + p(t). \tag{3.9}$$

Thanks to (3.8), we can also write:

$$U_e = -\frac{\phi}{1-\phi}U_c. \quad (3.10)$$

Substituting (3.10) in the fluid force balance in (3.1) leads to:

$$\frac{\phi}{1-\phi}U_c + \kappa(\phi-1)\frac{\partial P_e}{\partial r} = 0. \quad (3.11)$$

Exploiting (3.9), equation (3.12) can be formulated as well as:

$$\frac{\phi}{1-\phi}U_c + \kappa(1-\phi)\frac{\partial P_c}{\partial r} = 0. \quad (3.12)$$

which finally brings to:

$$\phi U_c = -(1-\phi)^2 \kappa \frac{\partial P_c}{\partial r}, \quad (3.13)$$

which is a Darcy-type equation for motion [6].

3.4 Non-Necrotic Model

The main assumption underlining these stages of growth is the constant cells volume ratio. Throughout these phases of expansion the region is assumed to be compact and the cell pressure must be greater than the fluid pressure to ensure strong cells bonds to keep the compactness (constant cell volume fraction $\phi = \phi_0$).

Initially there is a plentiful supply of oxygen which enables the proliferative phase to take place. The outer tumour boundary $X(t)$, defined through the condition of material surface

$$\frac{dX}{dt} = U_c, \quad (3.14)$$

moves towards the external tissue while cells are proliferating within the tumour, guaranteeing the expansion. The local oxygen concentration levels start to decay with time until in the center of the spheroid ($r = 0$) a critical threshold α ($0 < \alpha < 1$) is reached, giving origin to the apoptosis interface

$$r_c(t) : C(r_c, t) = \alpha \quad \forall t > t_1, \quad (3.15)$$

which separates the proliferative rim ($r_c(t) < r < X(t)$) from the apoptotic region ($0 < r < r_c(t)$).

Such a separation of proliferation from death is ulteriorly made clear with the definition of the net growth and death rate:

$$S(C) = \begin{cases} S_0 & \text{if } C > \alpha \\ -\rho & \text{if } C \leq \alpha \end{cases} \quad (3.16)$$

where S_0 is a constant value which describes the proliferation rate defined for oxygen levels above the critical threshold; whilst ρ is the constant taken for expressing how fast or how slow cells die defined when oxygen concentration levels start to become lower than α .

The oxygen consumption rate in (3.2) has been taken equal to a constant, namely $\Sigma(C) = \Sigma_0$, to achieve a simple computation of the oxygen concentration solution.

Setting the cells volume ratio equal to ϕ_0 , the dependent variables which characterise the proliferation and apoptosis phases are the cell pressure (related to the fluid pressure via (3.8) and to the cell radial velocity through (3.13)) and the oxygen local concentration.

The complete dimensional model for these stages of growth is:

$$\left\{ \begin{array}{ll} -\kappa \frac{(\phi-1)^2}{\phi} \frac{1}{r^2} \frac{\partial}{\partial r} \left(r^2 \frac{\partial P_c}{\partial r} \right) = \phi_0 S(C) & 0 < r < X(t) \\ \frac{\partial P_c}{\partial r} = 0 & r = 0 \\ P_c = p(t) & r = X(t) \\ D \frac{1}{r^2} \frac{\partial}{\partial r} \left(r^2 \frac{\partial C}{\partial r} \right) = \phi_0 \Sigma_0 & 0 < r < X(t) \\ \frac{\partial C}{\partial r} = 0 & r = 0 \\ C = C_0 & r = X(t) \end{array} \right. \quad (3.17)$$

where C_0 is the oxygen availability at the tumour boundary.

The boundary conditions at the tumour spheroid center are the typical no flux ones, given the symmetry; conversely, at the tumour border Dirichlet conditions have been imposed. In particular, the cell pressure at the tumour radius is equal to $p(t)$, which is usually given or considered as a function of the deformation of the external tissue, i.e. of tumour radius.

From (3.17), we can compute the dimensional solution for the oxygen concentration, which is:

$$C(r, t) = \frac{\phi_0 \Sigma_0}{6D} (r^2 - X(t)^2) + C_0 \quad (3.18)$$

The oxygen concentration attains the minimum in $r = 0$, as it can be seen in (3.18). During the proliferative phase, the value of such a minimum decreases with time because cells are uptaking nutrient for duplication: when the critical oxygen threshold defined in (3.16) is reached, apoptosis phase takes place in $r = 0$ and cells begin to die of nutrient starvation with an apoptotic rate ρ prescribed in (3.16) at the time instant $t_1 = \frac{3}{2} \log \left(\frac{6(1-\alpha)}{X_0^2} \right)$ (being X_0 the initial tumour radius). The tumour radius at which critical hypoxia ($C = \alpha$) is felt in the center of the spheroid is $X(t = t_1) = \sqrt{6(1-\alpha)}$.

In fig. (3.1) it is reported the oxygen concentration solution (the adimensional version which will be characterised later) plotted against the tumour radius for different time instants until the oxygen critical threshold α (set equal to 0.6 in the plots) is attained.

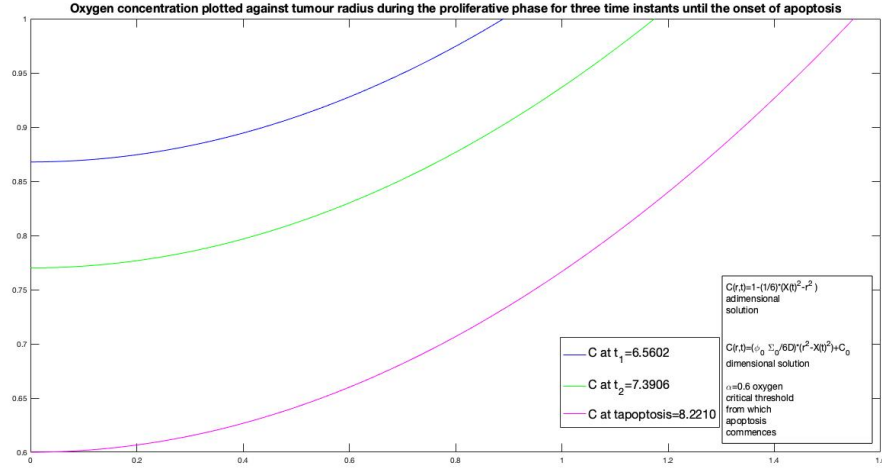


Figure 3.1: Local oxygen concentration plotted against tumour radius for some time instants for $\alpha = 0.6$.

3.5 Necrotic Model

As cells carry on proliferating in the proliferative rim ($r_c(t) < r < X(t)$) and dying of nutrient starvation in the apoptosis region ($0 < r < r_c(t)$), fluid pressure values in the latter region might increase such that they might become equal to cell pressure ones. In such a case, necrosis is achieved in $r = 0$, where the necrosis interface $L(t)$, subsequently defined, arises:

$$L(t) : P_c(L(t), t) = P_e(L(t), t) \quad (3.19)$$

In the necrotic region the hypothesis of constant volume ratio ceases to hold and the compactness is lost: the accumulation of the extracellular fluid make cells bonds weaker than in the compact region. A schematic representation of the tumour spheroid with the compacted and non-compacted region has been reported in fig. (3.2).

In the necrotic region, the compactness is lost, cells begin to float in the extracellular fluid ($U_c = U_e = 0$) and they are displaced by the progressive tumour expansion.

Thus the dependent variables employed to describe the necrotic phase are the cells volume fraction and and nutrient concentration.

In fact, the dimensional model is:

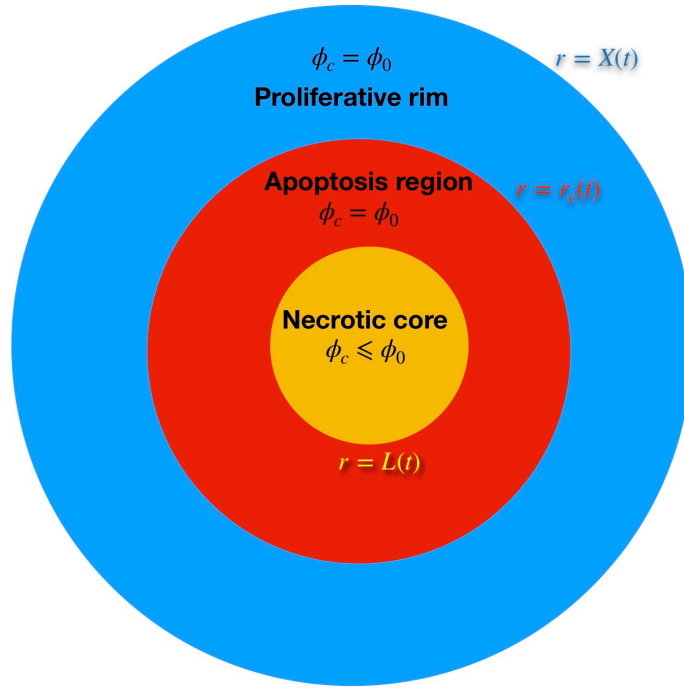


Figure 3.2: Schematic representation of the tumour spheroid when necrosis occurs.

$$\left\{ \begin{array}{ll} \frac{\partial \phi}{\partial t} = \phi S(C) & 0 < r < L(t) \quad \forall t > t_{necrosis} \\ \phi(t = t_{necrosis}) = \phi_0 & \\ D \frac{1}{r^2} \frac{\partial}{\partial r} \left(r^2 \frac{\partial C}{\partial r} \right) = \phi \Sigma_0 & 0 < r < L(t) \quad \forall t > t_{necrosis} \\ \frac{\partial C}{\partial r} = 0 & r = 0 \quad \forall t > t_{necrosis} \\ C(L^-, t) = C(L^+, t) & \forall t > t_{necrosis} \end{array} \right. \quad (3.20)$$

3.6 Non-dimensional Model

The subsequent non-dimensionalisation of the model has been made:

$$\begin{aligned} \Sigma(C) &= Q \bar{\Sigma}(C), \quad S(C) = S_0 \bar{S}(C), \quad C = C_0 \bar{C}, \quad \phi = \phi_0 \bar{\phi}, \\ \mathbf{x} &= \sqrt{\frac{DC_0}{\phi_0 Q}} \bar{\mathbf{x}}, \quad \mathbf{U}_c = S_0 \sqrt{\frac{DC_0}{\phi_0 Q}} \bar{\mathbf{U}}_c, \quad \mathbf{U}_e = S_0 \sqrt{\frac{DC_0}{\phi_0 Q}} \bar{\mathbf{U}}_e, \\ P_c &= \frac{DS_0 C_0}{Q \kappa (1 - \phi_0)^2} \bar{P}_c, \quad P_e = \frac{DS_0 C_0}{Q \kappa (1 - \phi_0)^2} \bar{P}_e, \quad p(t) = \frac{DS_0 C_0}{Q \kappa (1 - \phi_0)^2} \bar{p}(t), \end{aligned} \quad (3.21)$$

where the positive constants Q and S_0 are representative values for Σ and S , instead C_0 is the constant value of oxygen concentration on the outer boundary of the tumour. For the sake of brevity, the rescaled variables will be indicated without the above overbars. Physically we assume that the gel is highly permeable to extracellular fluid, thus allowing to set, without losing generality, at the tumour boundary the pore pressure equal to zero.

We can now re-write the equations in the two different regions, exploiting the spherical coordinates. In the compact region ($L(t) < r < X(t)$):

$$\frac{1}{r^2} \frac{\partial}{\partial r} \left(r^2 \frac{\partial C}{\partial r} \right) = \Sigma(C), \quad \phi = 1, \quad (3.22)$$

$$\frac{1}{r^2} \frac{\partial}{\partial r} (r^2 U_c) = -\frac{1}{r^2} \frac{\partial}{\partial r} \left(r^2 \frac{\partial P_c}{\partial r} \right) = S(C). \quad (3.23)$$

If necrosis occurs and then $L(t) > 0$, and the following continuity conditions must be respected at the necrotic interface $L(t)$:

$$[C]_-^+ = \left[\frac{\partial C}{\partial r} \right]_-^+ = \left[\frac{\partial P_c}{\partial r} \right]_-^+ = 0, \quad \text{at } r = L(t). \quad (3.24)$$

where the square brackets for a generic scalar function f of two independent variables stand for:

$$[f]_-^+ = f(L(t)^+, t) - f(L(t)^-, t) = \lim_{r \rightarrow L(t)^+} f(r, t) - \lim_{r \rightarrow L(t)^-} f(r, t). \quad (3.25)$$

In the necrotic region ($0 < r < L(t)$), then it holds:

$$\frac{1}{r^2} \frac{\partial}{\partial r} \left(r^2 \frac{\partial C}{\partial r} \right) = \phi \Sigma(C), \quad (3.26)$$

$$\frac{\partial \phi}{\partial t} = \phi S(C), \quad P_c = \frac{p(t)}{2}, \quad U_c = 0. \quad (3.27)$$

The boundary conditions for equations (3.22)-(3.23)-(3.26)-(3.27) are:

$$\frac{\partial P_c}{\partial r} = 0, \quad \frac{\partial C}{\partial r} = 0 \quad \text{at } r = 0, \quad (3.28)$$

$$C = 1, \quad P_c = p(t), \quad P_e = 0, \quad U_c = \frac{dX}{dt} \quad \text{at } r = X(t). \quad (3.29)$$

The initial boundary condition is: $X(0) = X_0 > 0$.

As already mentioned, we suppose that the gel is highly permeable to water, thus allowing the choice of the extracellular fluid pressure at the boundary.

Remarkable attention has to be posed, instead, to the cell pressure boundary condition, which signs one of the main differences with Landman and Please ([6]): in Chen et al. [2] cell pressure must balance with the outer tissue normal force, induced by tumour growth. In fact, Γ is the non-dimensional surface tension coefficient and $\sigma_{rr}(X, t)$ is the normal stress component of surrounding medium's stress tensor at the boundary of tumour $r = X(t)$. In Chen et al. model [2]

the outer tissue stress is characterized through a poro-elastic strain function, through which a tissue-momentum balance is written. Then the tumour and the outer tissue models are coupled via the boundary condition and solved together through a numerical method. In this piece of work, to investigate the influence of surroundings mechanics in the tumour spheroid readily, the tissue normal stress component is simply treated as an elastic force of varying stiffness acting on the tumour, as it will be seen in the subsequent section.

The cell pressure in the necrotic region (3.27) can be analysed through (3.9) and (3.19):

$$P_c = -P_e + p(t) \quad \underbrace{\Rightarrow}_{\text{Necrosis condition: } P_c=P_e} \quad P_c = \frac{p(t)}{2}. \quad (3.30)$$

Finally, to close the model, the kinetic terms $\Sigma(C)$ and $S(C)$ in (3.22)-(3.27) must be specified in the non-dimensional case. A simple approach has been preferred to carry out an analytical computation of the model ([6]):

$$\Sigma(C) = 1 \quad \text{and} \quad S(C) = \begin{cases} 1 & \text{if } C > \alpha, \\ -\rho & \text{if } C < \alpha, \end{cases} \quad (3.31)$$

where $0 < \alpha < 1$ is a critical oxygen threshold such that below it cells die of nutrient starvation with an apoptotic rate designed by ρ .

Chapter 4

Computation of the solution for the tumour model

The purpose of this section is to highlight the different effects caused by the surrounding medium on the tumour growth rate and size during the various stages of expansion.

Depending on the various constitutive laws taken into account for the external environment stress, there should be distinct scenarios for the tumour growth dynamics.

Chen et al. [2] imposed that at the tumour boundary there should be a balance between the cell pressure and the surface tension generated by the cells at the tumour border combined with the normal stress component of the outer tissue. In their simulations, they neglected the surface tension, and thus:

$$P_c(X(t), t) = p(t) = -\sigma_{rr}(X(t), t). \quad (4.1)$$

Characterising the surrounding medium through the strain energy function described in (2.4), Chen et al. connected the tumour and the outer tissue model via (4.1) and using a numerical method to solve them together.

However, at the present level, the normal stress component is treated as an elastic force acting on the tumour cells as follows:

$$\sigma_{rr}(X(t), t) = -\beta(X(t) - X_0),$$

where β can be considered as the tissue stiffness and X_0 the initial radius.

Looking at the tumour growth rate equation (3.14) and the structure of the kinetic terms (3.31), we can infer that the tumour growth dynamics is not influenced by the external stress during the nutrient rich and apoptosis phases.

The impact of the surrounding mechanical properties on the tumour growth rate and size can be observed once necrosis is initialised through the stated mechanical condition:

$$P_c(r, t) \leq P_e(r, t) \quad 0 \leq r \leq X(t),$$

namely when cells pressure is not strong enough to keep a compact structure of the tumour.

When necrosis occurs, instead, the tissue stiffness interferes with the dynamics of the external radius, since its evolution equation becomes:

$$3X^2 \frac{dX}{dt} = X^3 - (1 + \rho)r_c^3 + \rho L^3. \quad (4.2)$$

In turn, the necrosis radius is crucially influenced by the outer stress, since it stands (from a cell pressure continuity condition in at $L(t)$):

$$\frac{1}{2} \left(\frac{\Gamma}{X} - \sigma_{rr}(X, t) \right) - \frac{1}{3X} (X^3 - (1 + \rho)r_c^3 + \rho L^3) + \frac{1}{2} (X^2 - (1 + \rho)r_c^2 + \rho L^2) = 0. \quad (4.3)$$

As it can be seen in the above condition (4.3), it appears the necrotic interface L and the outer tissue normal stress component evaluated at the tumour boundary $\sigma_{rr}(X, t)$: this means that the necrotic interface is profoundly influenced by the outer stress and such influence is brought in the growth rate equation (4.2).

It's so clear the connection between the tumour dynamics and the tissue mechanical properties during this stage.

Besides the tumour expansion is independent of outer stress in the initial stages, and consequently of necrosis, it is reasonable to examine whether necrosis occurs or not or if it is delayed by changing the outer stress stiffness (β), the local oxygen threshold from which apoptosis commences (α), and the death rate (ρ).

4.1 Proliferative Phase

Initially the tumour is assumed to be small, non-necrotic and compact. Integrating equations (3.22)-(3.23) and exploiting the boundary conditions (3.28)-(3.29), we then have the following solutions with $\Sigma(C) = 1$:

$$C = 1 - \frac{1}{6} (X^2 - r^2), \quad (4.4)$$

$$U_c = -\frac{\partial P_c}{\partial r} = \frac{1}{r^2} \int_0^r y^2 S(C(y, t)) dy, \quad (4.5)$$

Seen the constraint of material surface given in the boundary condition (3.29), the expression of tumour growth rate is:

$$\frac{dX}{dt} = \frac{1}{X^2} \int_0^X y^2 S(C(y, t)) dy \quad (4.6)$$

The expression for the cell pressure can be easily obtained by integrating (4.5) by parts:

$$P_c = \left(\frac{1}{r} - \frac{1}{X} \right) \int_0^r y^2 S(y, t) dy + \int_r^X \left(y - \frac{y^2}{X} \right) S(y, t) dy - \sigma_{rr}(X, t). \quad (4.7)$$

During the early stage of the tumour, it can be assumed that there is a plentiful supply of oxygen, thus no programmed death occurs and we can consider that it holds $C > \alpha$ such that $S(C) = 1$. Hence, the shape of the solutions is:

$$C = 1 - \frac{1}{6} (X^2 - r^2), U_c = \frac{r}{3}, \quad (4.8)$$

$$X = X_0 e^{\frac{t}{3}}, \quad P_c = -\sigma_{rr}(X, t) + \frac{1}{6} (X^2 - r^2). \quad (4.9)$$

The value of $\sigma_{rr}(X, t)$ does not interfere with the tumour growth dynamics at the present stage, but it determines whether necrosis occurs or not.

According to these solutions, cells experience their highest compression in the center of the spheroid (i.e., the cell pressure maximum in $r = 0$), where cells uptake nutrient to grow and duplicate, driving the tumour expansion (seen the positive sign in the expression of the velocity field (4.8)).

4.2 Apoptosis and Necrotic Phase

With the progression of the expansion, $r = 0$ (the point at which local oxygen concentration attains the minimum) will be the first region to experience the dropping off of oxygen levels to the critical threshold α , leading to the apoptotic phase of the tumour growth.

The time at which significant death appears in $r = 0$, already introduced in (3.4), is:

$$t_1 = \frac{3}{2} \log \left(\frac{6(1-\alpha)}{X_0^2} \right), \quad (4.10)$$

attaining greater or lower values depending on how large the critical threshold α is (the greater it is, the faster apoptosis occurs), and how big the initial radius of the tumour X_0 is (the smaller it is, the later programmed death occurs given the stronger intercellular bonds which keep the ensemble together preventing more cells from death).

From this time instant, the apoptotic interface r_c defined in (3.15) arises, separating the proliferative rim ($r_c(t) < r < X(t)$) from the death region ($0 < r < r_c(t)$).

The interface r_c between live and dead cells can be also characterised in the following manner exploiting its definition (3.15) and the solution for the oxygen local concentration given in (4.4):

$$r_c^2 = X^2 - 6(1-\alpha) \quad \forall t > t_{apoptosis}. \quad (4.11)$$

The apoptotic interface interferes in the tumour growth dynamics, as it can be seen through the equation for the tumour growth rate (4.6), which written for this stage is:

$$3X^2 \frac{dX}{dt} = X^3 - r_c^3(\rho + 1). \quad (4.12)$$

Exploiting equations (4.5)-(4.7) and the continuity conditions of U_c , P_c and $\frac{\partial P}{\partial r}$ across the $r_c(t)$ interface, we gain the following solutions which hold true until necrosis occurs:

$$U_c = \begin{cases} -\frac{\rho r}{3}, & 0 < r < r_c(t), \\ \frac{1}{3r^2} (r^3 - (1+\rho)r_c^3), & r_c(t) < r < X(t), \end{cases} \quad (4.13)$$

$$P_c = \begin{cases} \frac{1}{6} (\rho r^2 + X^2) - \left(\frac{1+\rho}{2}\right) r_c^2 + \left(\frac{1+\rho}{3}\right) \frac{r_c^3}{X} - \sigma_{rr}(X, t) & 0 < r < r_c(t), \\ \frac{1}{6} (X^2 - r^2) - (\rho + 1) \frac{r_c^3}{3r} + \frac{r_c^3}{3X} (\rho + 1) - \sigma_{rr}(X, t) & r_c < r < X(t), \end{cases} \quad (4.14)$$

while, the local oxygen concentration solution does not change:

$$C = 1 - \frac{1}{6} (X^2 - r^2). \quad (4.15)$$

If no necrosis occurs, a non-necrotic steady state is consistent for tumour radius:

$$X(t) = X_\infty$$

where

$$X_\infty^2 = 6(1 - \alpha) \frac{(1 + \rho)^{\frac{2}{3}}}{(1 + \rho)^{\frac{2}{3}} - 1} > r_{c_\infty}^2 = \frac{6(1 - \alpha)}{(1 + \rho)^{\frac{2}{3}} - 1}, \quad (4.16)$$

which are obtained from setting to zero the right-hand side of the evolution equation (4.12). It is interesting to note that:

$$X^3 - (1 + \rho) r_c^3 = 0 \Leftrightarrow X = (1 + \rho)^{\frac{1}{3}} r_c = r_{P_{c_{max}}}. \quad (4.17)$$

The radius at which cell pressure attains the maximum comes to coincide with the expression of the steady state solution for the tumour boundary.

As r_c and X are both increasing functions of time, it is reasonable that the $r_{P_{c_{max}}}$ interface travels with time towards the outer boundary.

When the fluid pressure values increase until they reach those of cell pressure in $r = 0$, necrosis, instead occurs and the necrosis interface $L(t)$ arises and during time it separates two different regions: a compacted region occupying $L < r < X$ where both proliferation and death occur and a non-compacted necrotic region confined in $0 < r < L$.

Solution can be found through the equations (3.22)-(3.23)-(3.27) coupled with the boundary conditions (3.28)-(3.29) and the continuity conditions (3.24) across the necrotic interface $L(t)$.

Specifying the kinetic terms (3.31) Σ and S previously defined in (3.31), it is possible to show that the shape of the radial velocity component of the cell velocity field is:

$$U_c = \begin{cases} 0, & 0 < r < L(t), \\ -\frac{\rho}{3r^2} (r^3 - L^3), & L(t) < r < r_c(t), \\ \frac{1}{3r^2} (r^3 - (1 + \rho) r_c^3 + \rho L^3) & r_c(t) < r < X(t), \end{cases} \quad (4.18)$$

and for the cell pressure, we have:

$$P_c = \begin{cases} \frac{p(t)}{2} & 0 < r < L(t) \\ \frac{1}{6} (\rho r^2 + X^2) - \left(\frac{1+\rho}{2}\right) r_c^2 + \left(\frac{1+\rho}{3}\right) \frac{r_c^3}{X} + \frac{\rho L^3}{3} \left(\frac{1}{r} - \frac{1}{X}\right) - \sigma_{rr}(X, t) & L(t) < r < r_c(t) \\ \frac{1}{6} (X^2 - r^2) + \left(\frac{1}{r} - \frac{1}{X}\right) \left(\frac{\rho L^3}{3} - \left(\frac{1+\rho}{3}\right) r_c^3\right) - \sigma_{rr}(X, t) & r_c(t) < r < X(t) \end{cases} \quad (4.19)$$

Recalling the equations of the non-compact region (3.26)-(3.27), we have:

$$\begin{aligned} \frac{1}{r^2} \frac{\partial}{\partial r} \left(r^2 \frac{\partial C}{\partial r} \right) &= \phi, \\ \frac{\partial \phi}{\partial t} &= -\rho \phi, \end{aligned} \quad (4.20)$$

with the solution of the second equation for ϕ being

$$\phi = e^{-\rho(t-T(r))}, \quad (4.21)$$

where $T(r)$ is the time at which the necrotic condition $P_c = P_e$ is accomplished at the radius r .

We can now focus on the first equation of (4.20) for the local oxygen concentration:

$$\frac{1}{r^2} \frac{\partial}{\partial r} \left(r^2 \frac{\partial C}{\partial r} \right) = \phi. \quad (4.22)$$

Before integrating the above equation, given the solution found for the cell volume fraction (4.21), it is convenient to change the independent variable from r to T through the definition $r = L(T)$ (thus requiring that the necrotic interface $L(t)$ is an increasing function with time) previously written. Thus, we have:

$$\frac{1}{r^2} \frac{\partial}{\partial r} \left(r^2 \frac{\partial C}{\partial r} \right) = \frac{1}{L^2 L'} \frac{\partial}{\partial T} \left(r^2 \frac{\partial C}{\partial r} \right) = e^{-\rho(t-T(r))}. \quad (4.23)$$

Thanks to the no flux condition (3.28) at $r = 0$ for the oxygen concentration, we can integrate the preceding equation (4.23) from t_N (namely the time at which necrosis commences in $r = 0$) to $T(r)$:

$$r^2 \frac{\partial C}{\partial r} = \int_{t_N}^{T(r)} L^2 L' e^{\rho(\tau-t)} d\tau, \quad \text{for } 0 < r < L(t) \quad (4.24)$$

providing the flux condition at $r = L(t)$ for the solution of oxygen concentration in the compacted region (3.22) when necrosis occurs, which is then:

$$C = 1 - \frac{1}{6} (X^2 - r^2) + \frac{\rho}{3} \left(\frac{1}{r} - \frac{1}{X} \right) \int_{t_N}^{T(r)} L^3 e^{\rho(\tau-t)} d\tau, \quad \text{for } L(t) < r < X(t). \quad (4.25)$$

Chapter 5

Analysis and simulations

5.1 Proliferative phase

In fig. (5.1), it is reported the behaviour of cell and extracellular fluid pressures for $\beta = 0.08$ as elastic force stiffness during the proliferative phase until apoptosis occurs. During the initial time steps, there is a plentiful supply of oxygen which guarantees cells proliferation. Thus, cells start to proliferate driving tumour expansion and consequently the displacement $u = (X(t) - X_0)$ increases with time: the surrounding medium exerts a major compression over time on the tumour spheroid. As a consequence, cell pressures values at the boundary become greater with time, leading to a gradual separation from extracellular fluid pressures values and to a general increase of cell pressure values in the tumour inner regions. If a greater stiffness is chosen ($\beta = 0.8$ compared to $\beta = 0.08$), as in fig. (5.2), such a feature is accentuated. It is, in fact, clear how a different compression is reached at the tumour boundary, in particular, when apoptosis occurs, as shown in fig. (5.3).

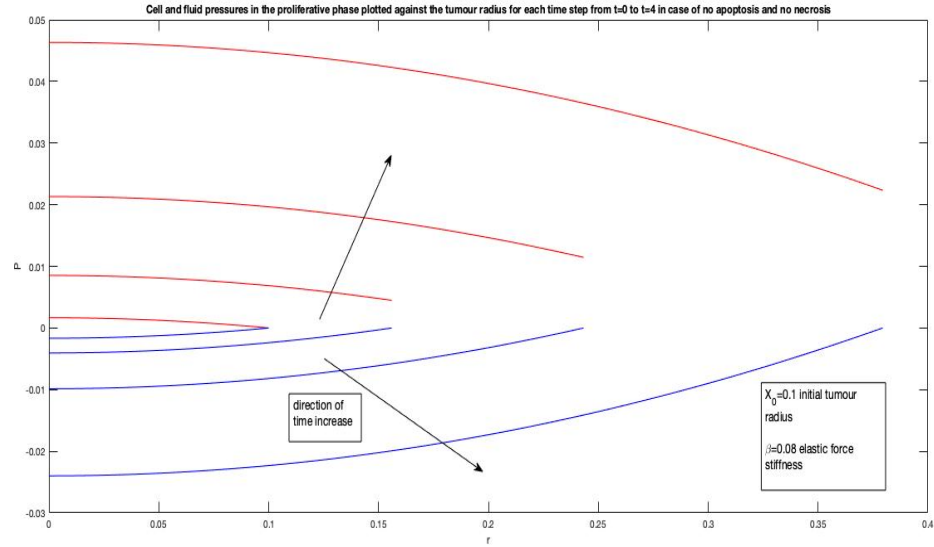
This peculiarity is even confirmed by the cell pressure maximum attained in $r = 0$, whose values are greater over time in the stiffer case, as it can be seen in fig. (5.4).

An equivalent alteration for varying the intensity of the elastic force acting on the tumour is changing the initial tumour radius, keeping the stiffness (β) fixed. If the tumour has an initial smaller size, the compressive forces are less intense during the initial stages of growth, as it can be noticed in fig. (5.5).

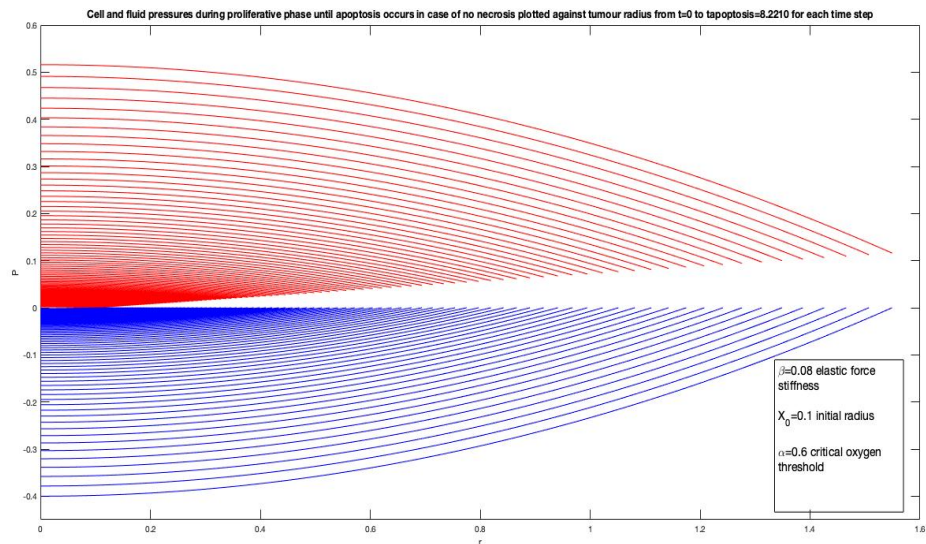
Reversely, when apoptosis phase is almost reached, the tumour sizes for the two different initial radii choices become comparable, and so the cell pressure values. It is remarkable to note, that, if the initial tumour size is smaller, the spheroid take more time to grow and to reach considerable dimensions, thus postponing the onset of apoptosis and the hypoxia experienced initially in the tumour center, as it can be detected in fig. (5.6).

In fact, recalling the local oxygen concentration solution for this stage of growth, it attains a minimum in the spheroid center, which over time decreases towards the critical threshold α , because of which programmed death begins accordingly to the net growth and death rate definition.

The evolution of the two tumour boundaries corresponding to the different choices for the initial radius is reported in fig. (5.7), again emphasizing how the initial difference in size leads to a different time for the onset of apoptosis.



(a) Evolution of cell and extracellular fluid pressure plotted against tumour boundary for each time step from $t_0 = 0$ for the first time instants for $\beta = 0.08$ elastic force stiffness.

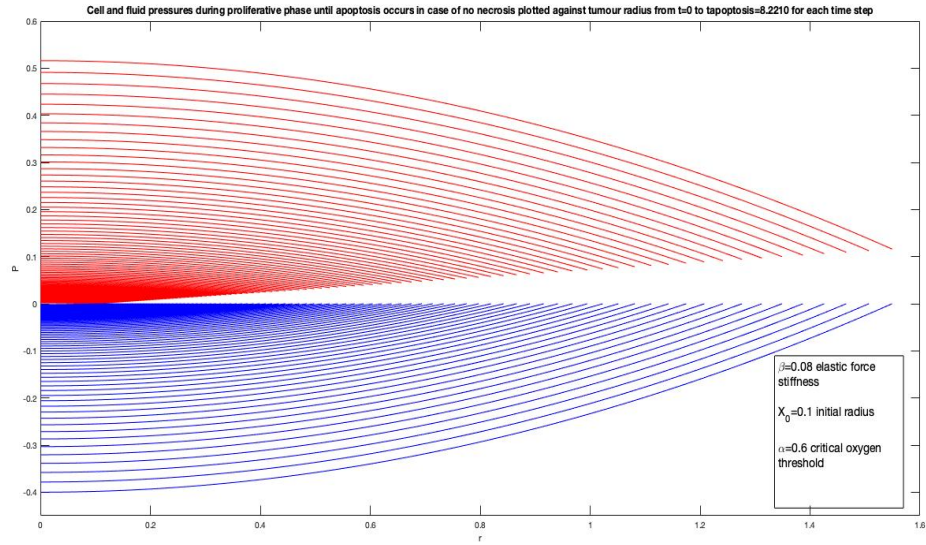


(b) Evolution of cell and extracellular fluid pressure plotted against tumour boundary for each time step from $t_0 = 0$ until apoptosis occurs for $\beta = 0.08$ elastic force stiffness.

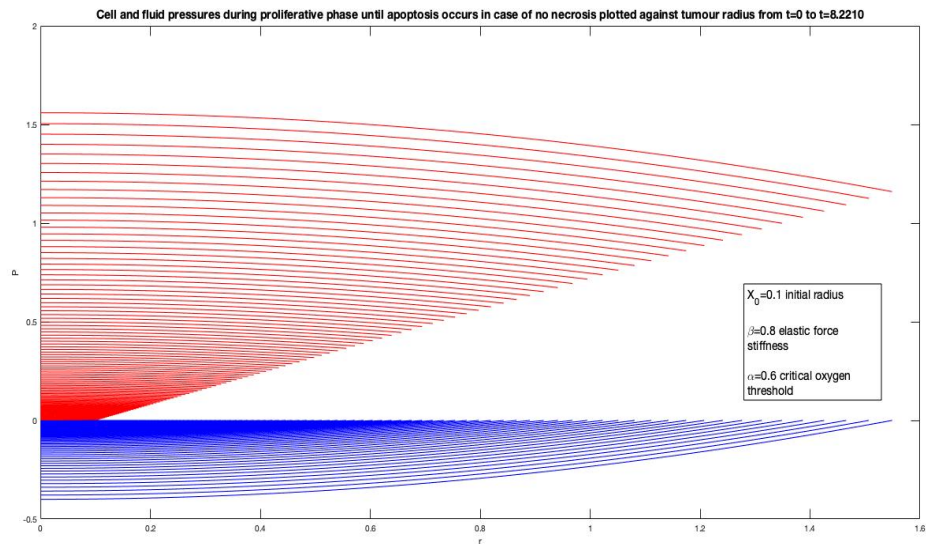
Figure 5.1: Evolution of pressures during the proliferative phase from the first time instants until apoptosis occurs for $\beta = 0.08$ elastic force stiffness. As the time goes on, the progressive displacement in the external tissue increases, thus leading to a greater compression felt by the tumour, in particular at the boundary. As it can be seen the value of the cell pressure at the tumour radius increases with time, bringing to a clear separation between cell and extracellular fluid pressures values.

5.2 Apoptosis Phase

Plots in fig. (5.8) describe how the general behaviour of both pressures varies from the proliferative phase to the apoptosis phenomenon.



(a) Evolution of cell and extracellular fluid pressure plotted against tumour boundary for each time step from $t_0 = 0$ until apoptosis occurs for $\beta = 0.08$ elastic force stiffness.



(b) Evolution of cell and extracellular fluid pressure plotted against tumour boundary for each time step from $t_0 = 0$ until apoptosis occurs for $\beta = 0.8$ elastic force stiffness.

Figure 5.2: Evolution of pressures during the proliferative phase from the first time instants until apoptosis occurs for $\beta = 0.08$ and $\beta = 0.8$ elastic force stiffnesses. In the stiffer case, the compression exerted by the external tissue is bigger: cell pressure values verge on major values and the separation from extracellular fluid pressure values is more evident than the less stiff case.

During the proliferative phase, intercellular forces are stronger in the center of the spheroid, gradually decreasing, instead, towards the tumour edges where new-born cells guarantee the tumour expansion. On the contrary, the extracellular fluid pressure experiences its lower values from $r = 0$ (where it attains the minimum) increasing instead outwards, where there is, in fact, more availability

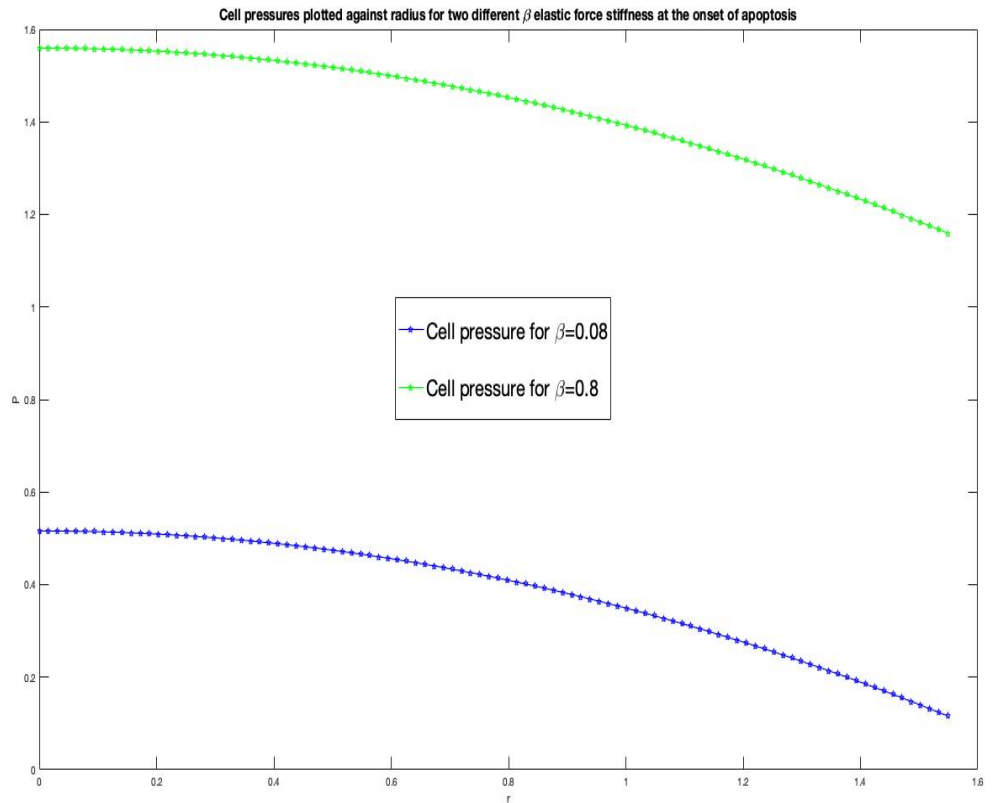
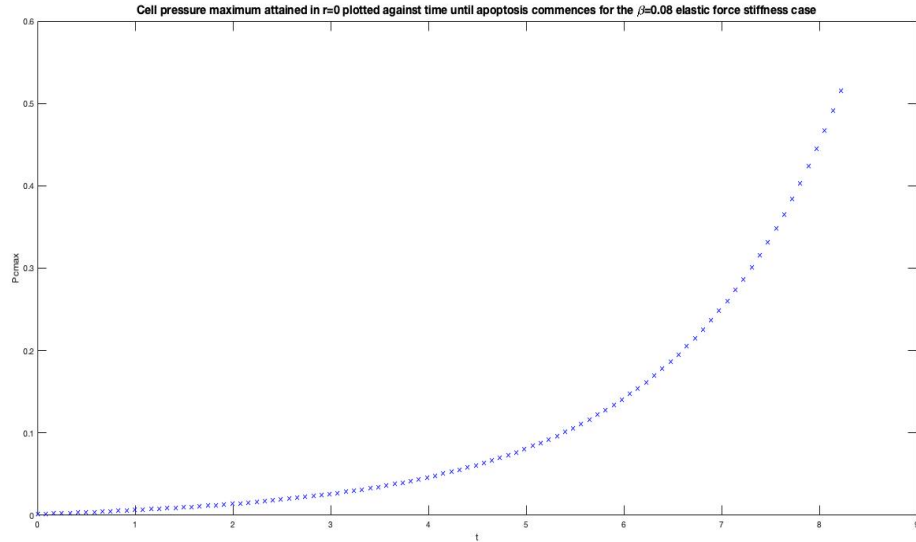


Figure 5.3: Cell pressures plotted against tumour boundary at the onset of apoptosis for the two different β choices. In green, we can see the cell pressure of the stiffer case reaching clearly larger values than the ones attained by the blue curve.

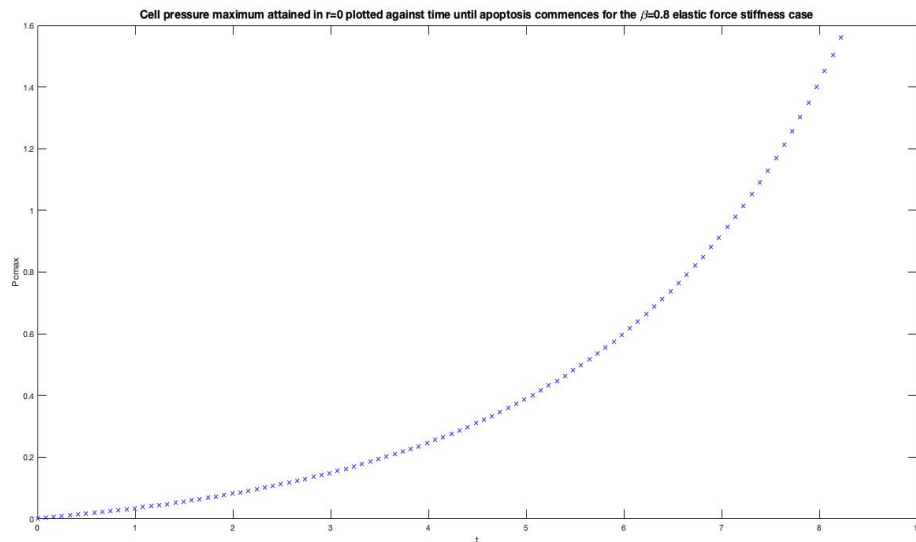
of nutrient (oxygen) uptaken by cells to duplicate.

When the critical oxygen threshold α (chosen to be equal to 0.6 in these simulations) is achieved, the apoptosis interface $r_c(t)$ arises in the center of the spheroid separating the region in which proliferation takes place ($r_c(t) < r < X(t)$) from the one where programmed death happens ($0 < r < r_c(t)$). Thus, the shape of pressures solutions change. In the center of the spheroid, cells while dying, release fluid, giving rise to an increase of extracellular fluid pressure values and to weaker cellular bonds of adhesion. Such a feature is kept while the apoptosis interface $r_c(t)$ travels with time. In the proliferative region, instead, the tendency of the solutions is similar to the one described in the previous phase of growth.

For such a $\beta = 1.5$ choice no necrosis occurs, as it can be seen in fig. (5.9). The external compression is powerful enough to make the cell pressure value at the boundary increase with time. Stronger external compressions bring the cell pressure to higher values in the tumour inner regions, leading again to a clear separation with extracellular fluid pressure values. Moreover, the $r = r_{P_{c_{max}}} = (1 + \rho)^{\frac{1}{3}} r_c(t)$ interface, where P_c attains the maximum, creates two different regions in which a reverse mechanical attitude can be spotted.



(a) Cell pressure maximum attained in $r = 0$ plotted over time until apoptosis occurs for $\beta = 0.08$ case.



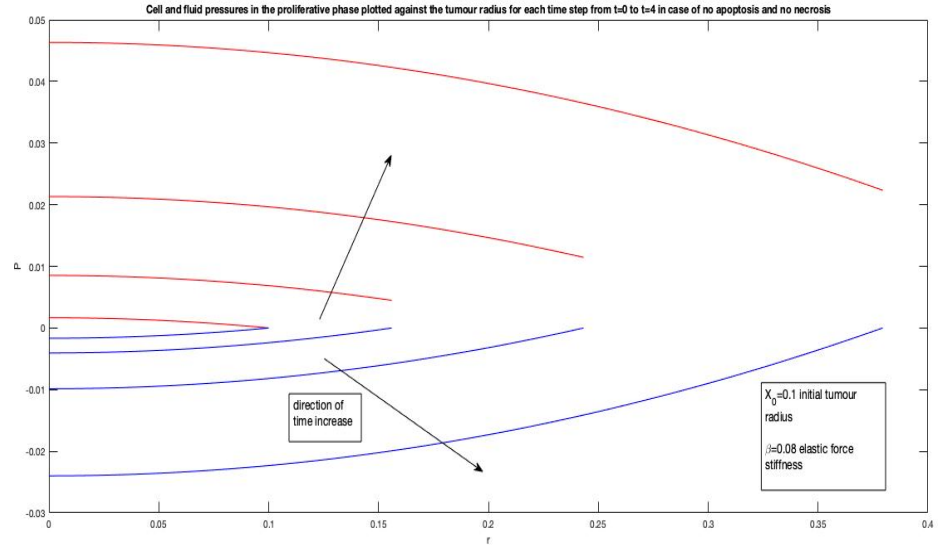
(b) Cell pressure maximum attained in $r = 0$ plotted over time until apoptosis occurs for $\beta = 0.8$ case.

Figure 5.4: Comparison of cell pressure maximum values over time for two different β choices ($\beta = 0.08$ and $\beta = 0.8$). The stiffer case shows how larger values are reached over time.

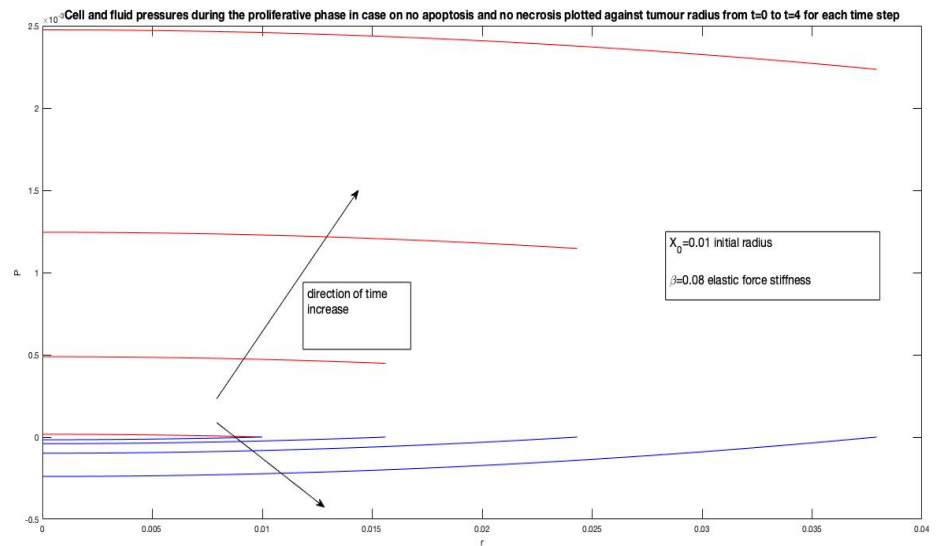
For $r > r_{P_{c_{max}}}$, to ensure expansion, as the tumour boundary is still an increasing function of time, cells tend to go outwards. For this reason, cell pressure decreases with radius where the tumour is expanding.

On the contrary, for $r < r_{P_{c_{max}}}$ cells move towards the center of the spheroid guarantee the constraint of constant volume fraction.

Under this external tissue stiffness, the compressive forces become very powerful over time, and, thus, cell migration is even more impeded, leading the $r_{P_{c_{max}}}$



(a) Evolution of cell and extracellular fluid pressure plotted against tumour boundary for the first time instants for $\beta = 0.08$ elastic force stiffness and $X_0 = 0.1$ initial tumour radius.

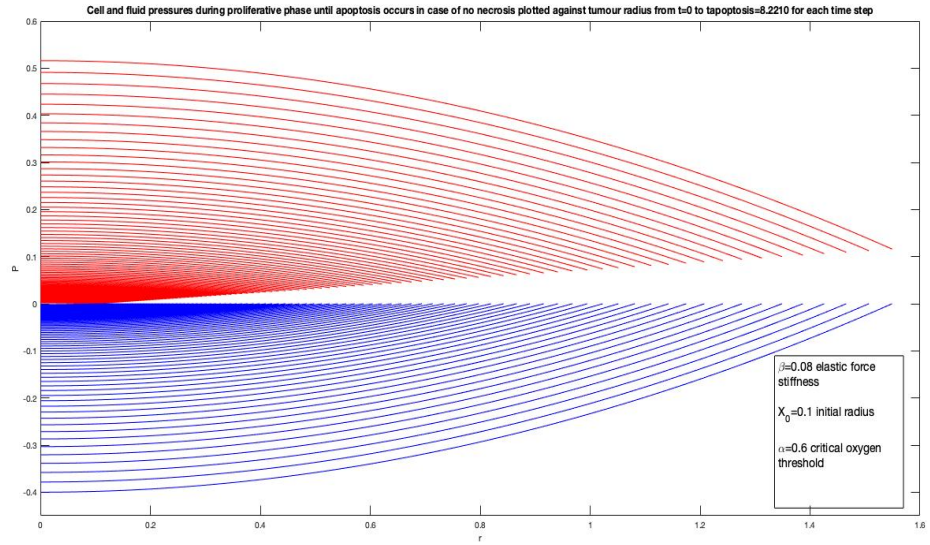


(b) Evolution of cell and extracellular fluid pressure plotted against tumour boundary for the first time instants for $\beta = 0.08$ elastic force stiffness and $X_0 = 0.01$ initial tumour radius.

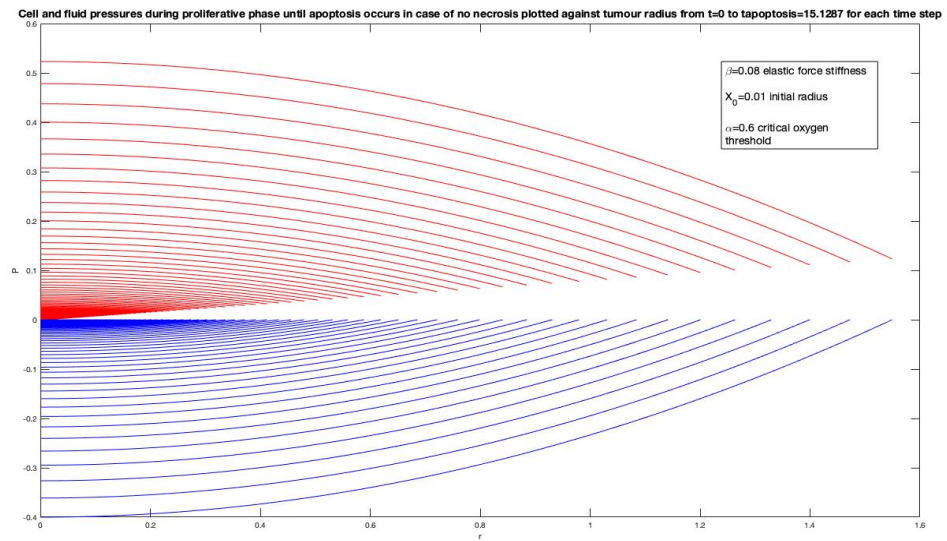
Figure 5.5: Evolution of pressures during the proliferative phase for the first time instants for $X_0 = 0.1$ and $X_0 = 0.01$ initial tumour radii, being $\beta = 0.08$. In the $X_0 = 0.01$ scenario, the tumour has an initial tumour radius one order of magnitude minor than the other case. Consequently, the tumour spheroid has much smaller sizes during the first time instants, originating weaker compressive forces. Cell pressure values differ from one order of magnitude.

interface to a progressive accumulation of cells, bringing the $P_{c_{max}}$ on higher values, as it can be observed clearly in the time instants plotted in fig. (5.10).

The tumour and apoptosis interfaces are then reported in fig. (5.11) during their evolution in the proliferative and apoptosis phases.



(a) Evolution of cell and extracellular fluid pressure plotted against tumour boundary for each time step from $t_0 = 0$ until the onset of apoptosis for $\beta = 0.08$ elastic force stiffness and $X_0 = 0.1$ initial tumour radius.



(b) Evolution of cell and extracellular fluid pressure plotted against tumour boundary for each time step from $t_0 = 0$ until the onset of apoptosis for $\beta = 0.08$ elastic force stiffness and $X_0 = 0.01$ initial tumour radius.

Figure 5.6: Evolution of pressures during the proliferative phase until the onset of apoptosis for $X_0 = 0.1$ and $X_0 = 0.01$ initial tumour radii, being $\beta = 0.08$. In the $X_0 = 0.01$ scenario, the time at which apoptosis commences is achieved much later by the tumour aggregate compared to the greater initial radius choice.

It is of remarkable importance to outline even for this stage of growth what kind of features arises with the tumour initial radius variation, keeping instead the stiffness (β) fixed.

Varying the tumour initial radius entails two different times for the onset of apoptosis.

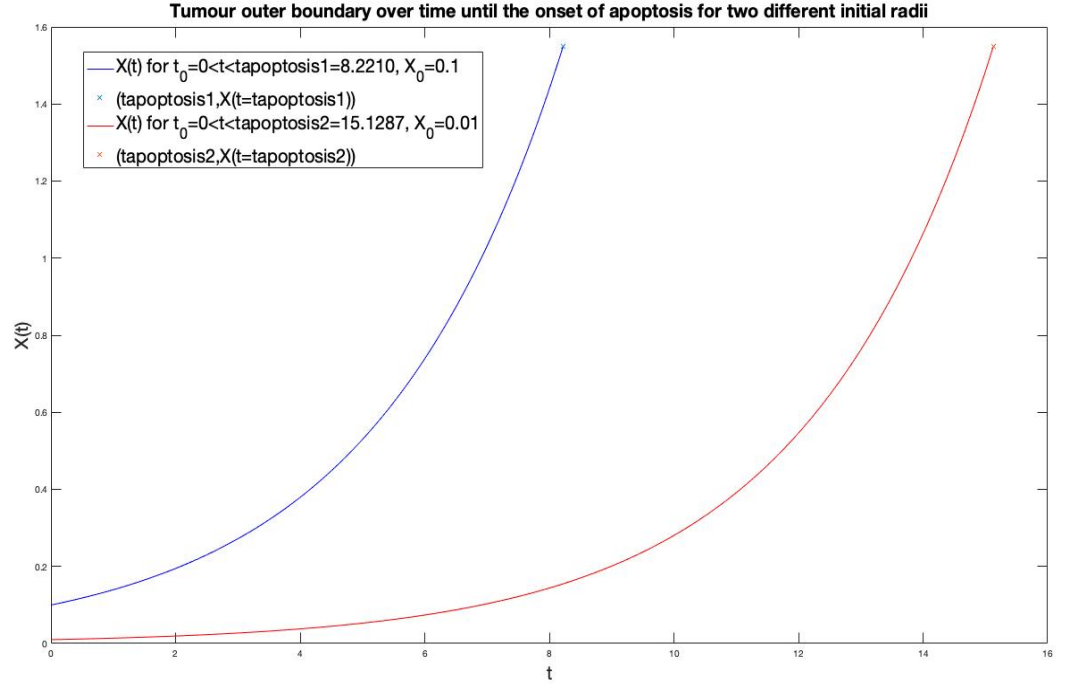


Figure 5.7: Outer tumour interfaces over time until apoptosis commences for two different choices of initial tumour radius.

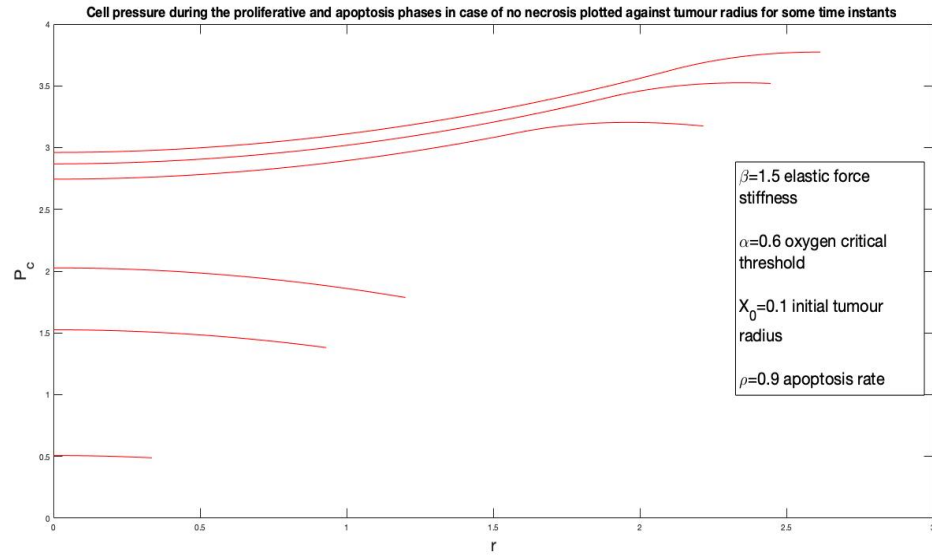
Choosing $X_0 = 0.01$ as initial tumour radius, combined with $\beta = 1.5$ elastic force stiffness choice conducts again to a non necrotic scenario.

It is interesting to note that the behaviour of the two cell pressures corresponding to the different choices of initial tumour radius in fig. (5.2). Both cell pressures are plotted against the tumour radius at the last time instant of the time interval chosen for the simulations (i.e., $t_{final} = t_{apoptosis} + 12$): cell pressure values corresponding to the $X_0 = 0.01$ choice are greater than the non-variated case. Also, cell pressure maximum, attained in the proliferative rim, has over time (even if the onset of apoptosis is different for $X_0 = 0.01$ choice), during the apoptosis phase, greater values than the ones attained in the other scenario.

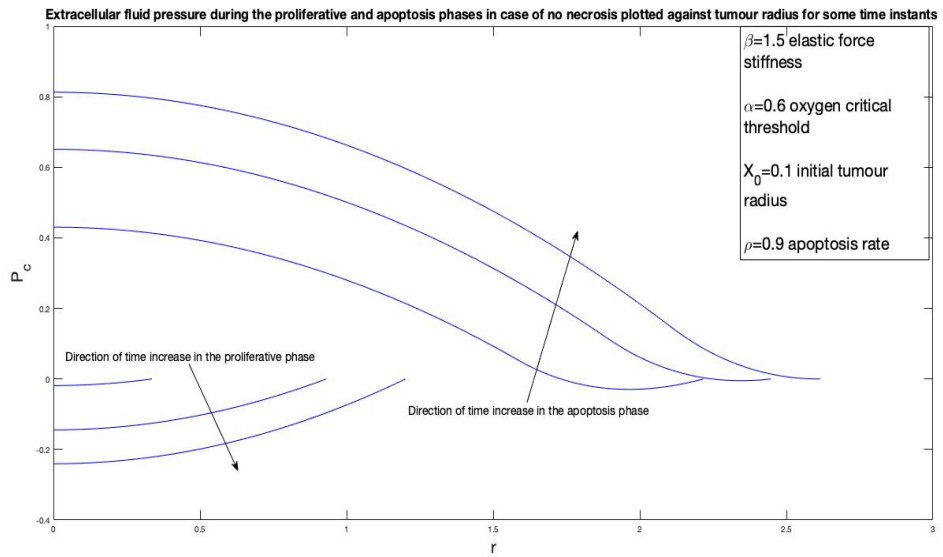
If we go back in the proliferative phase, as shown in fig. (5.12), cell pressure values reached at $t = 4.0690$ and $t = 8.2210$ (time of onset of apoptosis for $X_0 = 0.1$ case) of the lower initial tumour radius are smaller.

When apoptosis is reached also for the $X_0 = 0.01$ case, the corresponding cell pressure values become greater than the ones of $X_0 = 0.1$ scenario at the onset of apoptosis, as shown in fig. (5.13).

Such a behaviour can be explained by the fact that, initially, the tumour sizes for the $X_0 = 0.01$ scenario are very much smaller compared to the $X_0 = 0.1$ case. For this reason, the progressive displacement in the external tissue will be less at these initial stages, leading to weaker compressive forces and lower cell pressure values in the proliferative phase. The time at which apoptosis commences is delayed in the $X_0 = 0.01$ scenario: $t_{apoptosis_2} = 15.1287 > t_{apoptosis_1} = 8.2210$. In general, the tumour radius at which apoptosis is initiated is $X(t = t_{apoptosis}) =$



(a) Evolution of the cell pressure during the proliferative and apoptosis phase plotted against tumour boundary for some time instants for $\beta = 1.5$ elastic force stiffness in a non necrotic scenario



(b) Evolution of the extracellular fluid pressure during the proliferative and apoptosis phase plotted against tumour boundary for some time instants for $\beta = 1.5$ elastic force stiffness in a non necrotic scenario

Figure 5.8: Evolution of cell and fluid pressures during the proliferative and apoptosis phases in case of no necrosis for $\beta = 1.5$. The tissue stiffness is strong enough to guaranteeing an increase of cell pressure values with time from the outer boundary to inner regions of the proliferative rim.

$\sqrt{6(1-\alpha)}$, independent of the initial tumour radius X_0 . Therefore, the tumour radius at $t_{apoptosis} = 15.1287$ for the $X_0 = 0.01$ choice will be the same of the $X_0 = 0.1$ case at $t_{apoptosis} = 8.2210$, but the displacement in the surrounding medium $u = (X(t = t_{apoptosis}) - X_0)$ will be considerably greater for the $X_0 = 0.01$ scenario, provoking the increase of the external compressive forces. Such an

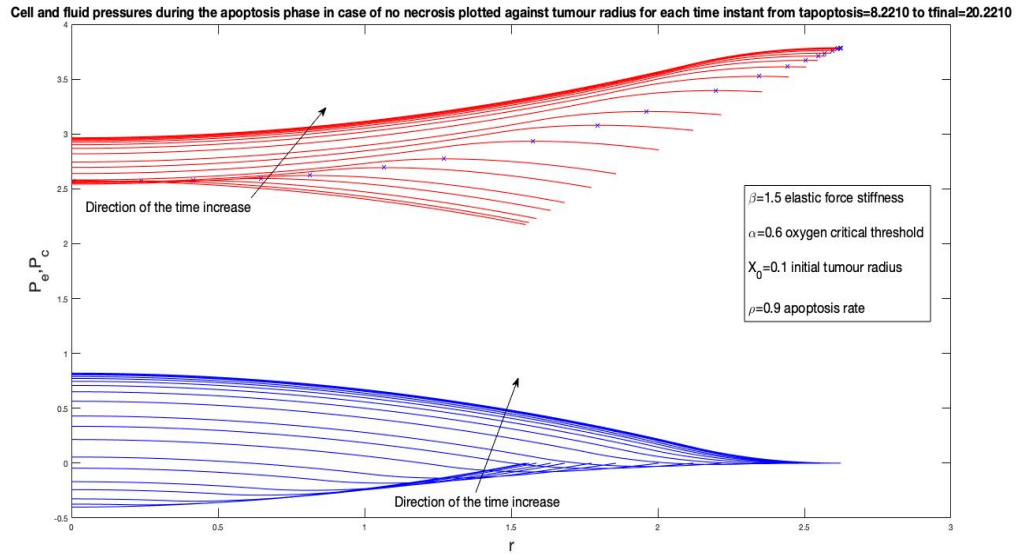


Figure 5.9: Evolution of cell and extracellular fluid pressures during the apoptosis phase in case of no necrosis for $\beta = 1.5$.

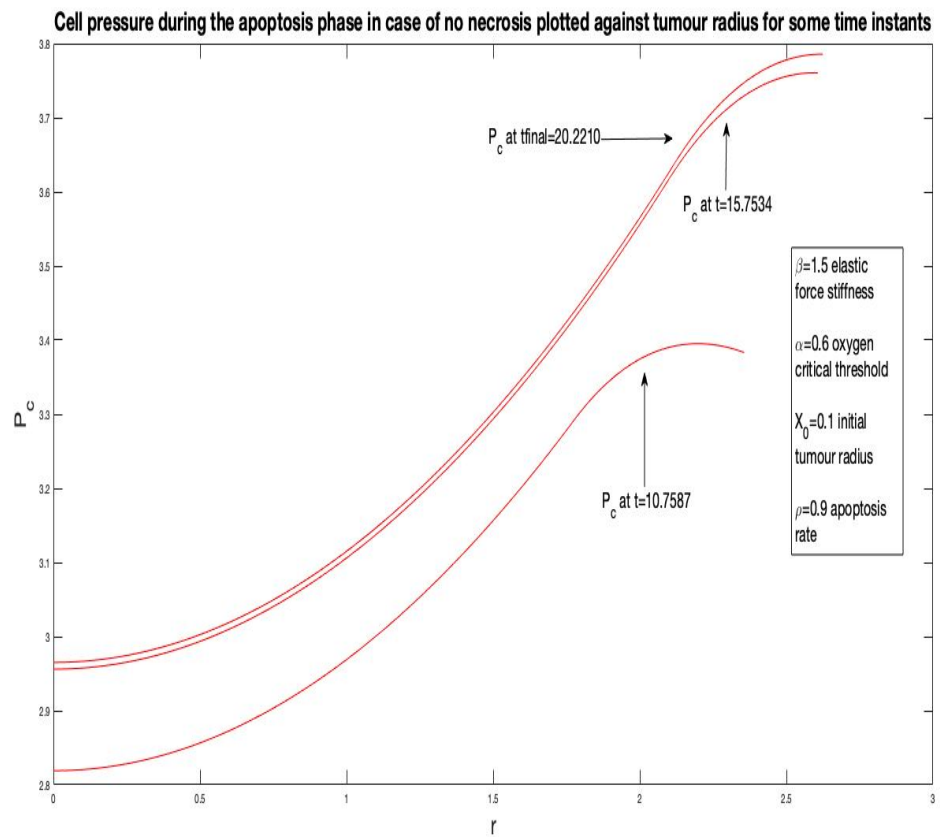


Figure 5.10: Cell pressure plotted against tumour radius at some time instants in the apoptosis phase for $\beta = 1.5$. As the time passes, cell pressure verges on larger values.

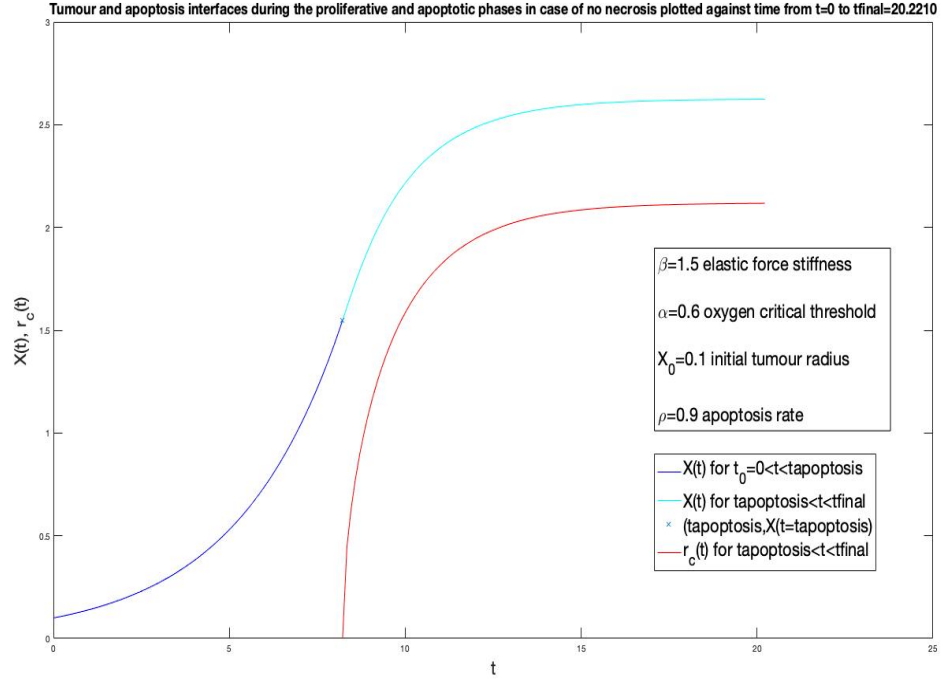


Figure 5.11: Evolution of tumour and apoptosis interfaces with time during proliferative and apoptosis phases in case of no necrosis for $\beta = 1.5$.

increase accounts for the cell pressure greater values in the $X_0 = 0.01$ scenario during the apoptosis phase.

5.3 Apoptosis phase with the onset of necrosis

Choosing lower values for the β elastic force stiffness causes the weakening of intercellular bonds and consequently the increase of extracellular fluid pressure values, until, in the center of the spheroid ($r = 0$), the necrosis condition ($P_c = P_e$) is satisfied, as it can be seen in fig. (5.14)-(5.15)-(5.16)-(5.17).

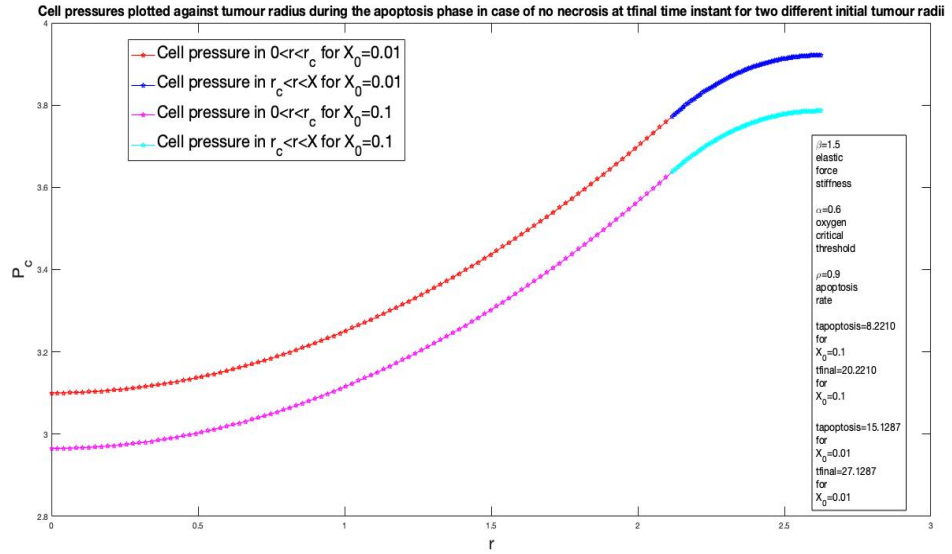
The most remarkable feature of the aforesaid graphics is how to a decrease of the external tissue stiffness (β) corresponds an anticipation of necrosis time.

We can now focus on the $\beta = 0.05$ scenario and analyze some interesting characteristics.

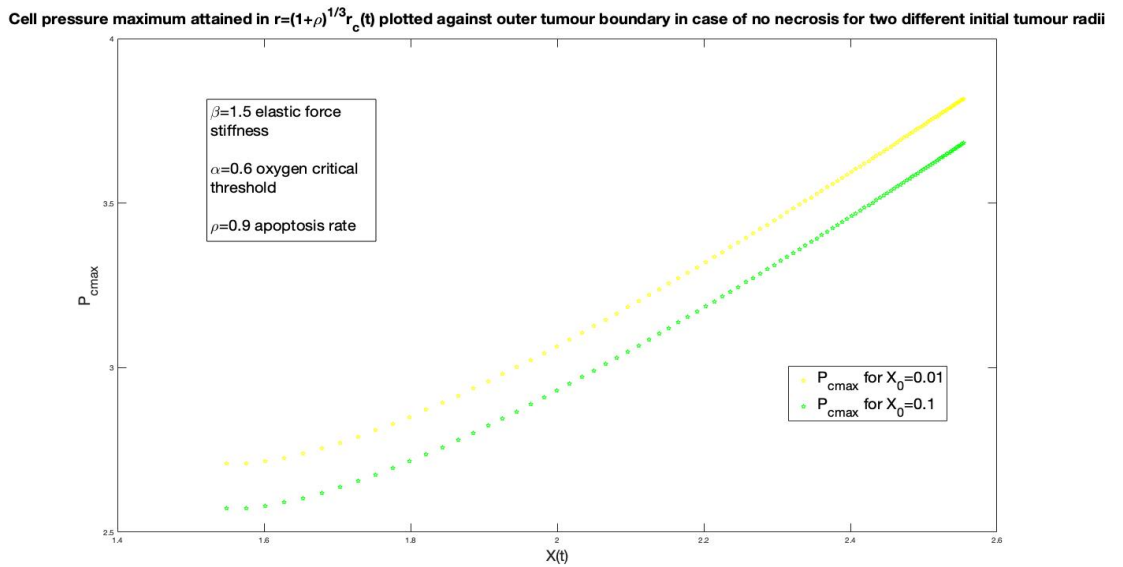
In fig. (5.18) it is reported more specifically how necrosis is reached in such a stiffness case, by plotting the cell and extracellular fluid pressures just for some time instants including the curves that mark the triggering of necrosis in $r = 0$.

In fig. (5.19), for the same β scenario, tumour and apoptosis interfaces have been inserted in their evolution during the proliferative and apoptosis phase until necrosis is attained.

If we keep the stiffness (β) fixed, we can play with the oxygen critical threshold α parameter as well to see how the onset of necrosis is anticipated or retarded according to its variations.



(a) Cell pressures plotted against tumour radius at last time instant chosen for the simulations of the apoptosis phase for $\beta = 1.5$ corresponding to the two different initial tumour radius ($X_0 = 0.01$ and $X_0 = 0.1$) choices in a non necrotic scenario.



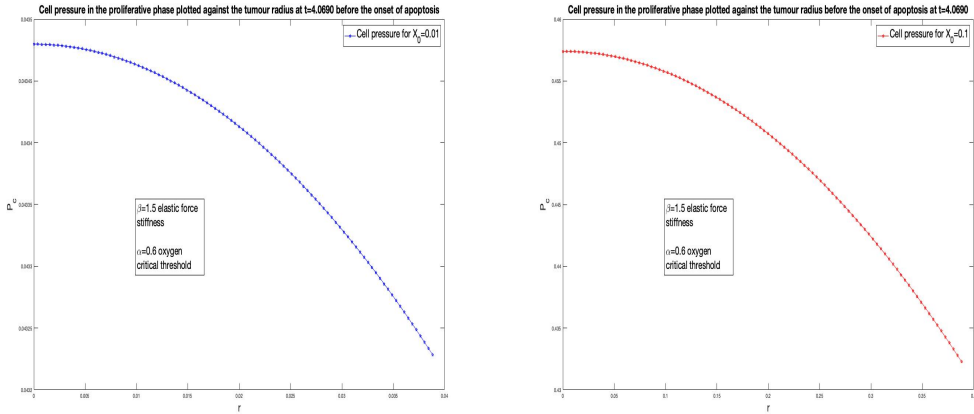
(b) Cell pressure maximum plotted against tumour boundary for each time step of the two different apoptosis phases corresponding to the diverse choices of initial tumour radius

Intuitively, for example, if we increase the value of such a parameter (α) from 0.6 to 0.7, it takes less time for the oxygen concentration to attain the critical value and enhancing the beginning of apoptosis. In other words, under the same stiffness, changing the α parameter to a greater one, means anticipating the onset of apoptosis and consequently of necrosis.

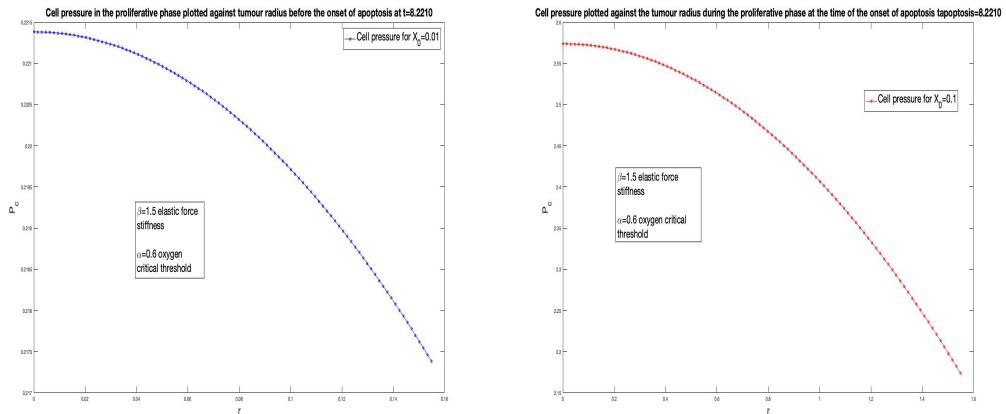
As evidence, two series of plots have been added.

m

In fig. (5.20) the tumour and apoptosis interfaces are reported in their evolution over time during the proliferative and apoptosis phases until necrosis is



(a) Cell pressure during the proliferative phase before the onset of apoptosis plotted against tumour radius at $t=4.0690$ for $\beta = 1.5$ and $X_0 = 0.01$ (b) Cell pressure during the proliferative phase before the onset of apoptosis plotted against tumour radius at $t=4.0690$ for $\beta = 1.5$ and $X_0 = 0.1$



(c) Cell pressure during the proliferative phase before the onset of apoptosis plotted against tumour radius at $t=8.2210$ for $\beta = 1.5$ and $X_0 = 0.01$ (d) Cell pressure during the proliferative phase plotted against tumour radius at $t_{apoptosis}=8.2210$ for $\beta = 1.5$ and $X_0 = 0.1$

Figure 5.12: Cell pressures plotted against tumor radius for different time instants for $\beta = 1.5$ corresponding to the two different initial tumour radius choices $X_0 = 0.1$ and $X_0 = 0.01$.

reached for both α choices. As predicted, the starting times for apoptosis and necrosis in the $\alpha = 0.6$ option are preceded by those of the other parameter value. The magenta line in fig. (5.20), which represents the apoptosis interface for $\alpha = 0.7$, appears and vanishes earlier in time, marking anticipated apoptosis and necrosis, as the green line, which stands for the outer tumour boundary for $\alpha = 0.7$, terminates before the blue line (the tumour border for the other scenario), signaling the earlier outset of apoptosis.

In fig. (5.21), we can detect the different behaviour kept by both the pressures for the two different α scenarios. In the higher α choice, a major decrease of the cell pressure in the apoptosis region can be spotted, given the fact that the apoptosis phenomenon had taken place earlier. In fact, being $\alpha = 0.7$ com-

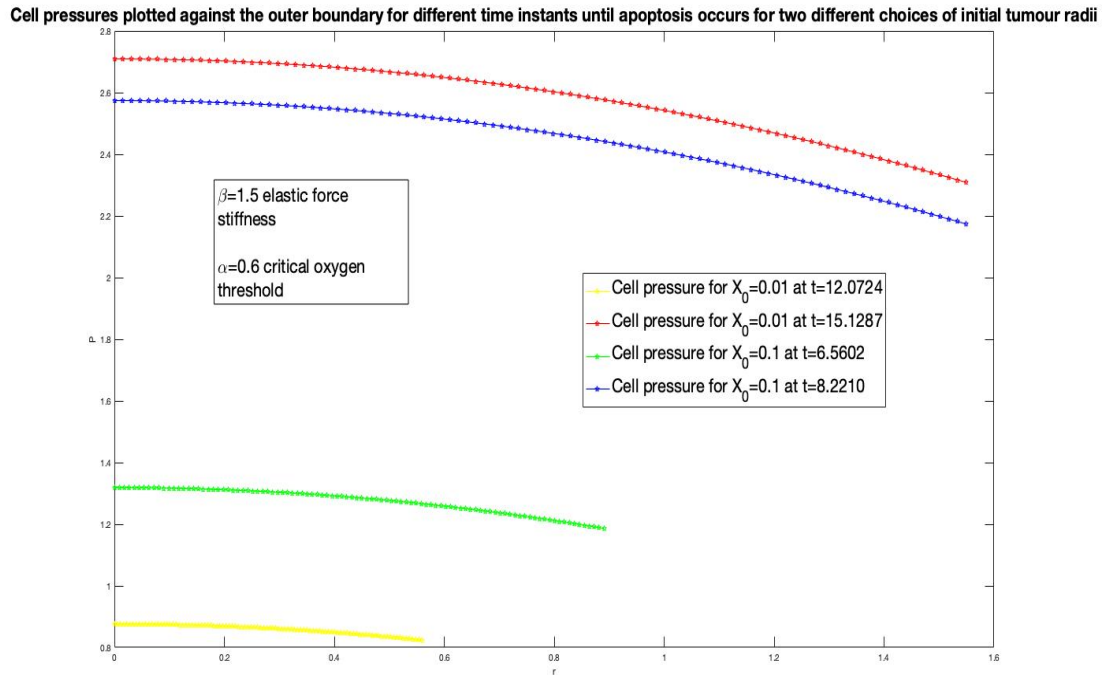


Figure 5.13: Cell pressures plotted against tumour radius for different time instants in the proliferative phase before the onset of apoptosis for $\beta = 1.5$ corresponding to the two different initial tumour radius choices $X_0 = 0.01$ and $X_0 = 0.1$

pared with $\alpha = 0.6$, it means that there is less availability of nutrient for cells duplication: less cells are able to duplicate and to drive tumour expansion and the apoptosis is then reached readily. To keep the constraint of constant volume fraction in this kind of scenario, it implies that cells should increase in size, then the number cell density would be lower and intercellular bonds weaker. Such an attitude would explain the cell pressure lower values for the $\alpha = 0.7$ case, even though this modelling framework is pretty simplified and it is not really able to detect cell single behaviours.

A last interesting characteristic to be also analysed in this section is the behaviour of cell pressure maximum in the apoptosis phase if necrosis is spotted. As we can see in fig. (5.22), lowering the stiffness, the maximum tends to decrease over time until necrosis is reached, and the shape of the solution changes. In case of β lower values, compressive forces are indeed weaker compared to β greater values, and so are the intercellular forces. If such compressive forces are not so strong to keep a powerful structure of the ensemble of cells, cells migration is eased in comparison with major compressive scenarios. For this reason, the $r_{c_1 P_{c_{max}}}$ interface goes through a progressive loss of cells: cells which move towards the boundary to drive expansion and other inwards to keep the compactness of the spheroid structure.

What happens, instead, increasing the stiffness, gives rise to a different kinetic attitude, as it is shown in fig. (5.23): progressively widening the values of β , we

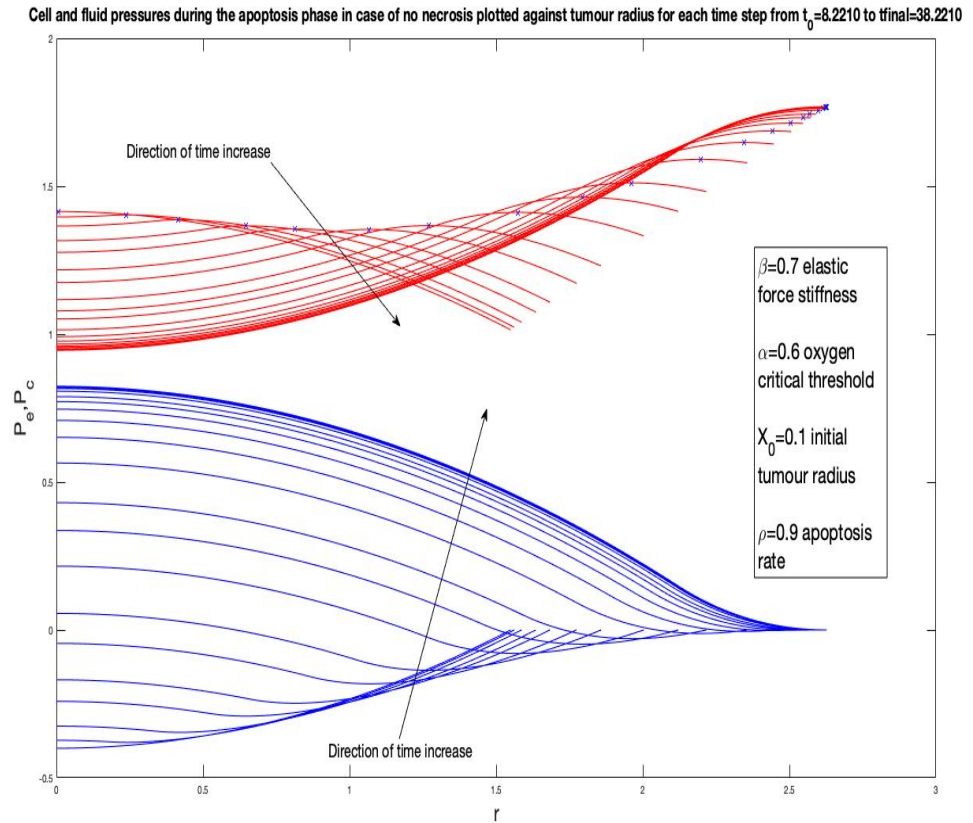


Figure 5.14: Cell and fluid pressures during the apoptosis phase in case of no necrosis appearance for $\beta = 0.7$ and $X_0 = 0.1$. The arrows indicate the direction of time increase. Differently from the $\beta = 1.5$ in the apoptosis without necrosis occurring in (5.2), cell pressure values start from higher values and, in the apoptotic region ($0 < r < r_c(t)$), they tend to decrease with time seen the minor stiffness of the external tissue ($\beta = 0.7$ vs. $\beta = 1.5$). Even if extracellular fluid pressure values are increasing in the apoptotic region, no necrosis here occur because a non-necrotic steady state is reached in the tumour boundary (as it can be spotted in the last time instants cell pressure curves) and the values for both the pressures stabilize.

can observe a clear augmentation of cell pressure values over time, especially in the non-necrotic cases, which strong intercellular forces prevent the tumour aggregate from entering in the necrosis phase. In such scenarios compressive forces are very powerful to guarantee a massive robust structure of the spheroid and so cell migration, instead, here, is made harder over time. Indeed, the $r_{c|P_{cmax}}$ interface experiences a gradual accumulation of cells (being the maximum achieved in the proliferative rim) which leads to greater P_{cmax} values over time. Probably cells reduce their sizes to maintain the same volume ratio as the lower *beta* cases, even if, as already mentioned before in this section, we are not able to detect it under this simplified modelling framework.

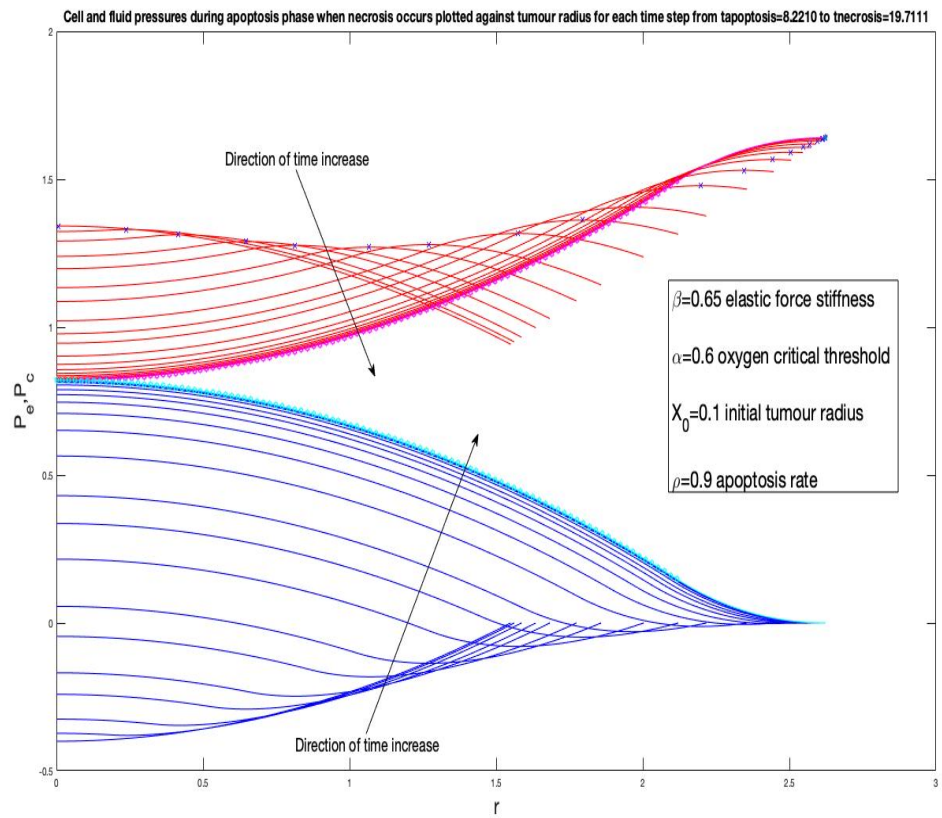


Figure 5.15: Cell and fluid pressures during the apoptosis phase in case of necrosis appearance for $\beta = 0.65$ and $X_0 = 0.1$. The arrows indicate the direction of time increase. Decreasing the elastic force stiffness of 0.05 ($\beta = 0.65$ vs. $\beta = 0.7$), necrosis here occurs.

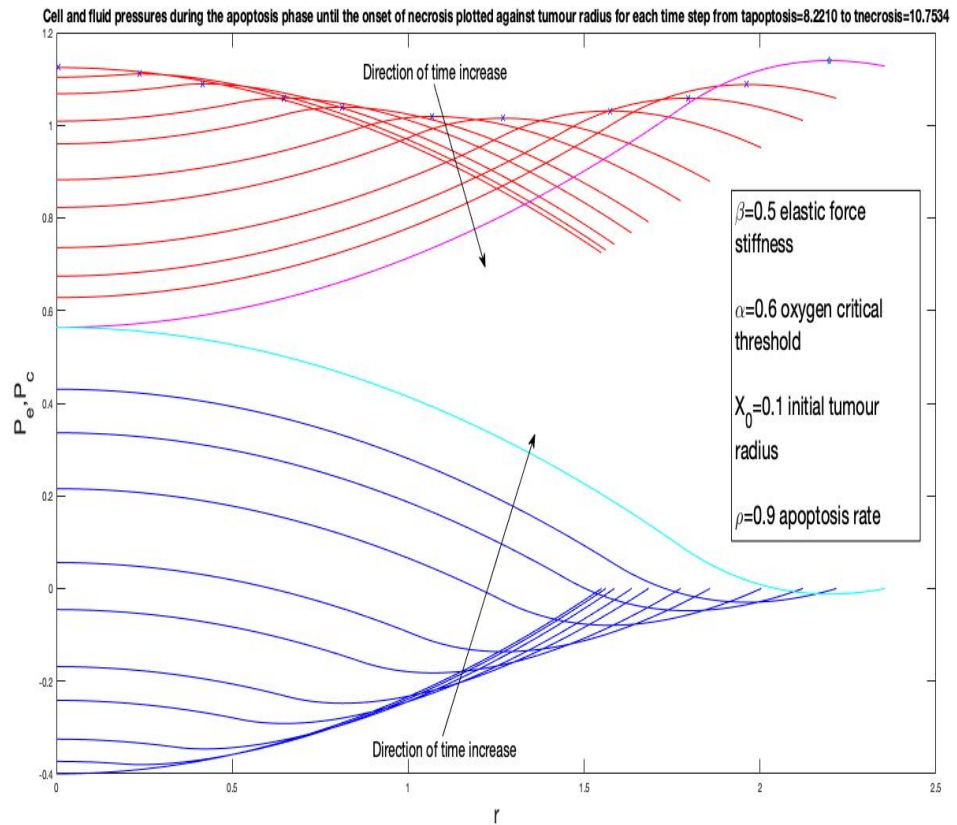


Figure 5.16: Cell and fluid pressures during the apoptosis phase in case of necrosis appearance for $\beta = 0.5$ and $X_0 = 0.1$. The arrows indicate the direction of time increase. Decreasing the elastic force stiffness β , the onset of necrosis is anticipated. As we can see, the cell pressure values in the apoptosis region rapidly decrease with time, given the weakening of intercellular bonds, until the necrosis condition ($P_c = P_e$) is readily achieved in $r = 0$ by the two pressures.

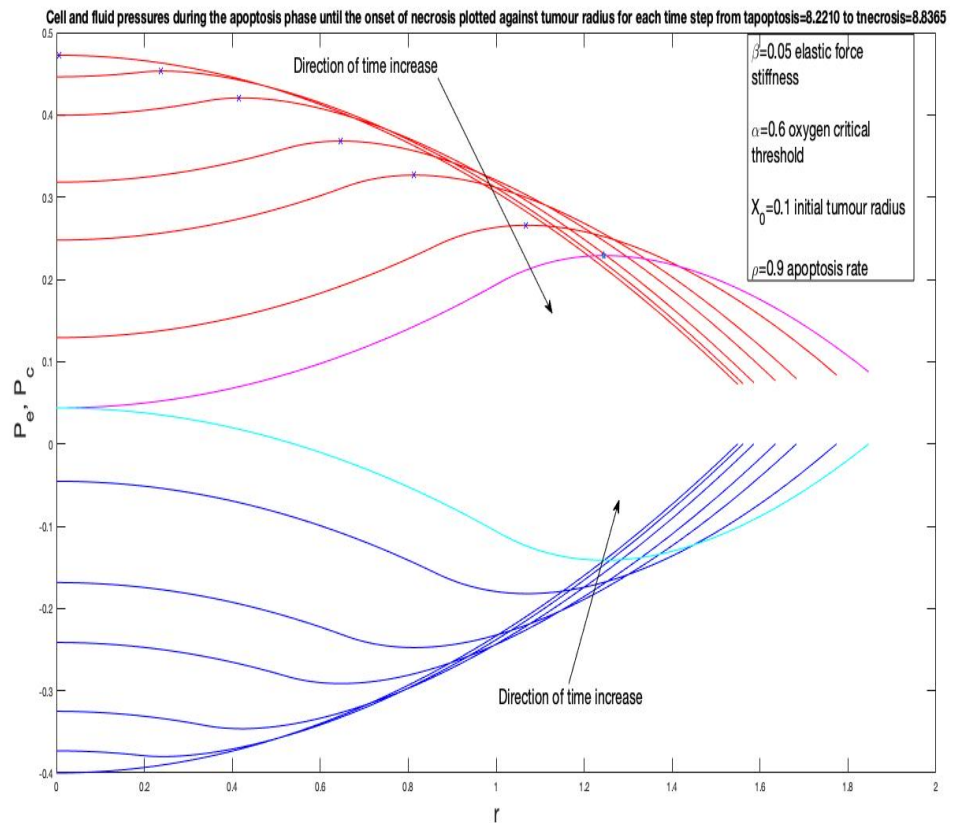


Figure 5.17: Cell and fluid pressures during the apoptosis phase in case of necrosis appearance for $\beta = 0.05$ and $X_0 = 0.1$. The arrows indicate the direction of time increase. Decreasing the elastic force stiffness β of one order of magnitude in respect of the preceding case (fig. (5.16)), the decrease of cell pressure values in the apoptosis region is much accentuated and the necrosis is attained faster than the $\beta = 0.5$ case.

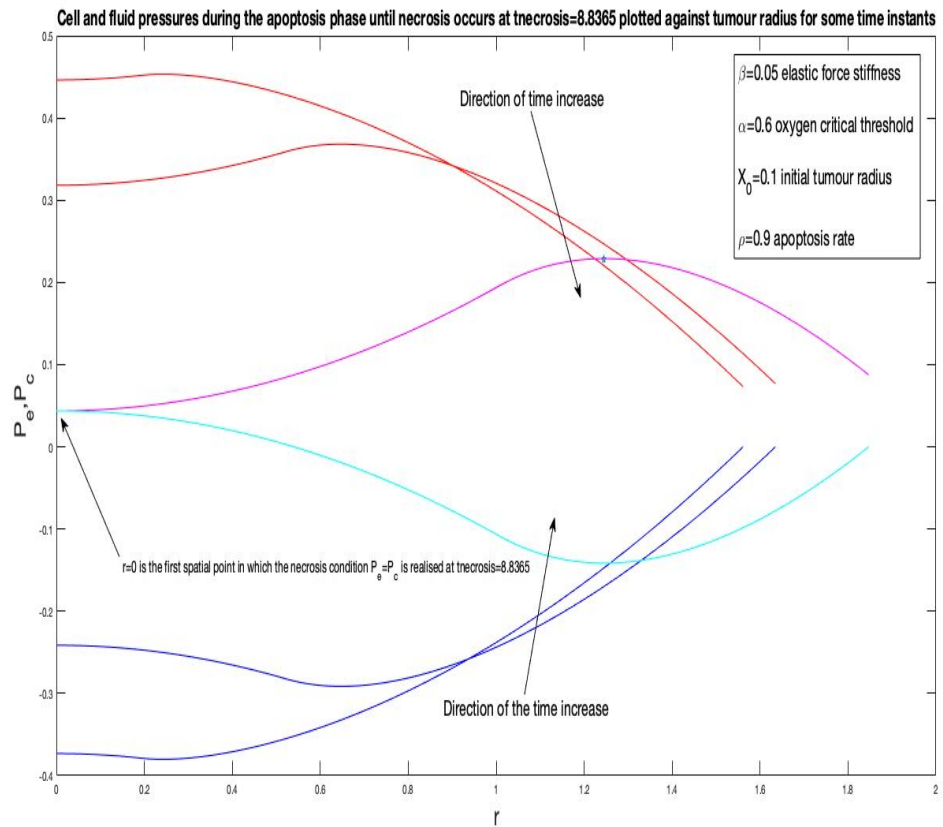


Figure 5.18: Graphics of cell and fluid pressures for the $\beta = 0.05$ stiffness case against tumour radius for some time instants, with a particular focus to the necrosis time. The magenta and cyan curves for the cell and fluid pressure respectively represent the last solution for the pressures in the apoptosis phase, starting from which the necrosis phase is initialized.

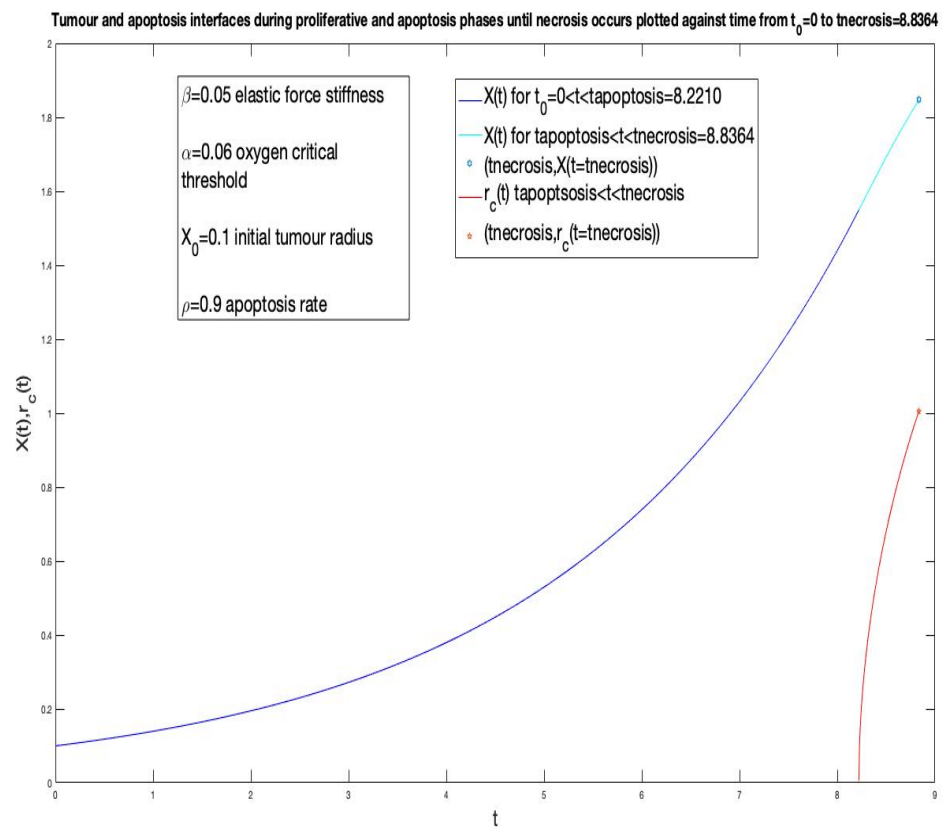


Figure 5.19: Tumour and apoptosis interfaces in their evolution with time for the proliferative and apoptosis phases and the apoptosis phase respectively until necrosis commences, for the $\beta = 0.05$ case.

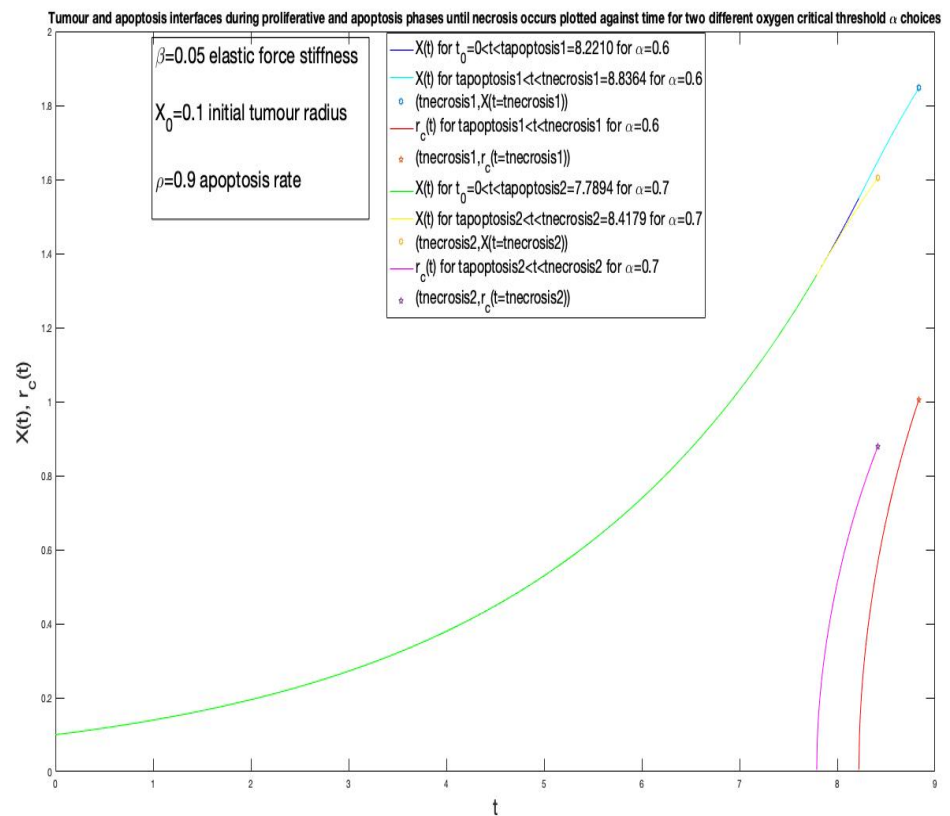


Figure 5.20: Tumour and apoptosis interfaces plotted over time during the proliferative and apoptosis phases until necrosis occurs for $\alpha = 0.6$ and $\alpha = 0.7$.

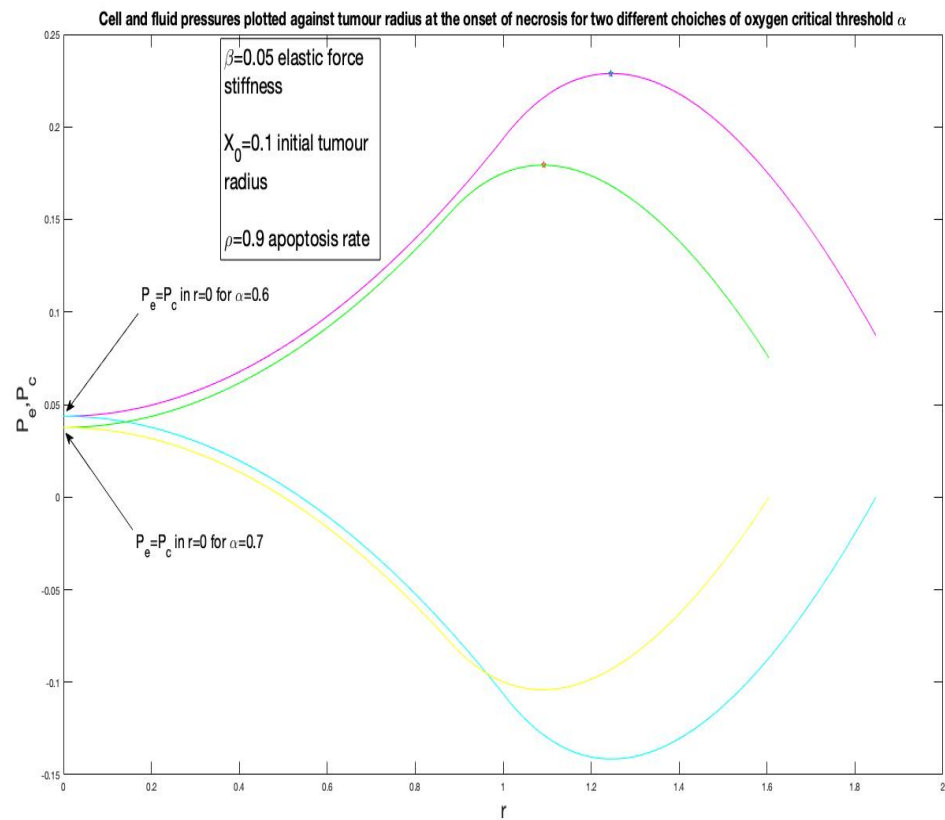


Figure 5.21: Cell and fluid pressures plotted against tumour radius at the necrosis time for each α choice ($\alpha = 0.6$ - $\alpha = 0.7$).

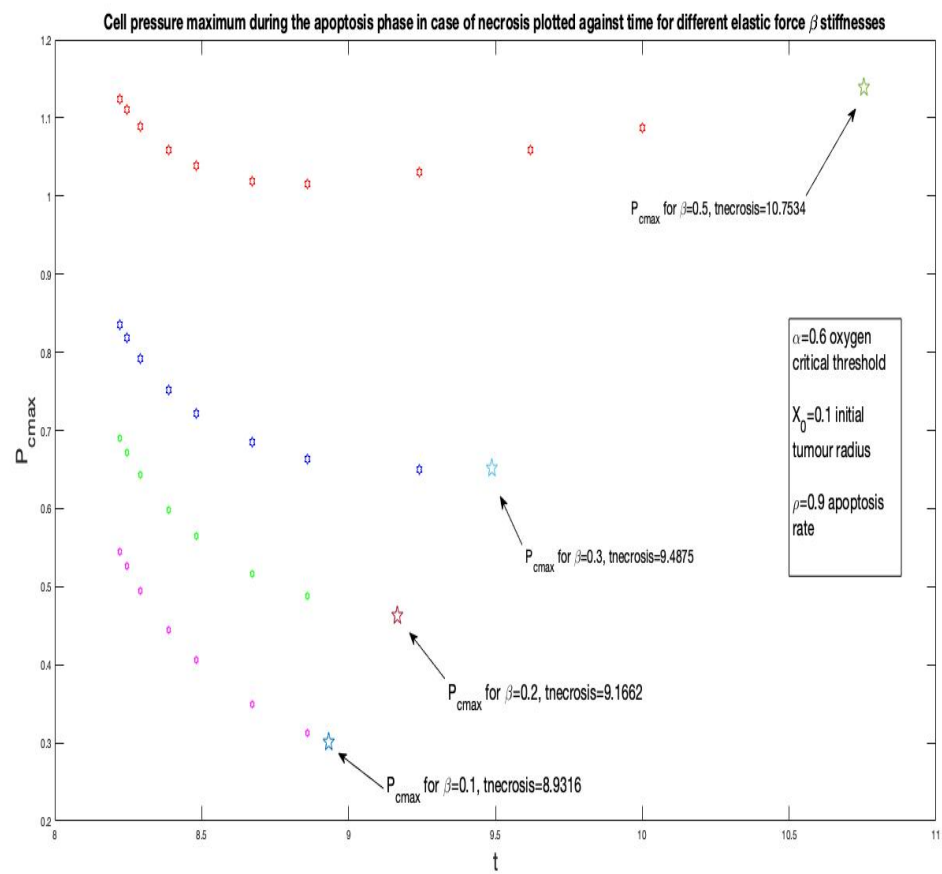


Figure 5.22: Behaviour over time of cell pressure maximum in case of necrosis for different stiffnesses β values during apoptosis phase.

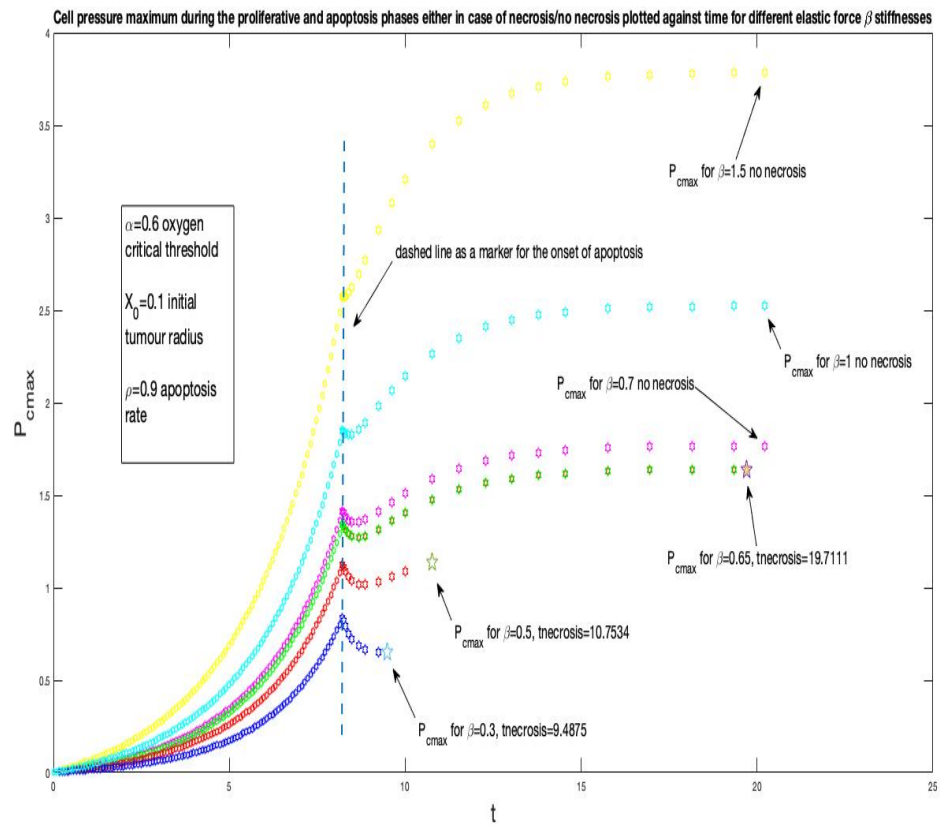


Figure 5.23: Behaviour over time of cell pressure maximum either in case of necrosis/no necrosis for different stiffnesses β values during apoptosis phase.

Conclusions

In this piece of work, much analysis has been devoted on how the growth induced stress affects tumour growth during the various stages of expansion, by treating the external medium as an elastic force at the boundary.

Interesting features have arisen by varying the elastic force stiffness in every phase of growth. Increasing the external tissue stiffness means giving the tumour a more compact structure, seen the simultaneous increase of the intercellular forces. It is of pivotal importance to understand critically how such strengths are weakened or reinforced by the external stress: a more compact and powerful structure confers a survival advantage to the tumour. Indeed, increased compaction, as caused by the external surrounding medium, or as found in the tumour spheroid inner layers, triggers a multicellular-dependent mechanism of increased radiation resistance [17] and both intrinsic and acquired drug resistance [18]. To analyse more precisely how the surrounding medium mechanics influences the tumour aggregate dynamics and kinetics would be better to consider a non-isotropic stress field. Also, the next crucial step would be adding a mechano-sensitive property, in order to make tumour growth dynamics dependent on the outer stress also during the proliferative and apoptosis phases and not only once necrosis is begun. Thus, the model could capture how the microscopic cellular parameters vary according to the alterations in the structure of the external tissue stress. Such compressive forces would influence the tumour growth rate from the initial stages of expansion and not only when necrosis is triggered.

Understanding what kind of macroscopic and microscopic features might change given a particular outer stress field through a more accurate model would help in characterising accurately the growth-induced tumour inhibition detected in Helmlinger experiments [1].

Such improvements might also help in raising the efficacy of some medical treatments and therapies, leading to a significant awareness of the tumour future evolution.

Acknowledgments

The achievement of this master dissertation is the sum of enormous little steps made during the duration of the degree course and the abroad thesis experience in Oxford.

This work might be considered as a starting experience for upgrading and improving my skills levels in one of my greatest passions in life: mathematical modelling applied to cancer. From a mathematical and biological perspectives, it would have been done way more difficult than it has been made here, to investigate more deeply and consciously some features, but I am profoundly thankful to everything that has arisen from this experience. I was supervised by one of the most incredible scientists I could ever wish for as supervisors Helen Byrne and Luigi Preziosi, from whom I have also learned how would like to become one day in my future career as a researcher. They were always there ready to listen to every single idea came to my mind, and their feedbacks, the possibility to interact with them deepening a vast list of mathematical biology topics constituted a precious present which has enriched my scientific mindset enormously. I have to thank them endlessly for every single help they gave me for the production of this dissertation.

The experience in Oxford as a background in my everyday life during the development of this work was magical. I have discovered a sort of unreal world where all the things that you could not believe would have been possible came to life. This tiny town pushes your limits to be best you can try to achieve in every aspect of your daily life.

The years spent in Turin were crucial for my personal growth, helping me to understand what kind of future pathways I would have liked to cross or begin and the type person I hope to become in the future gradually.

Everything I listed was possible only thanks to the most important people in my life: my parents, my best friends. They have always taught me that everything I wanted to reach could be attained with hard work, intense passion, and humbleness. There were more moments in which I did not believe in myself enough, and I thought I was not as good as the standards requested by the degree course I was attending. They were there to support me, allowing every experience I needed for my future and never making me feel weak, even in my failures. I would not be the person I am today without their teachings, support and giant love.

Also, every person, every new friend I made during these years was crucial for building every single piece of the current myself. With their help, different perspectives enriched my way of seeing things in life and their company was a relief in the saddest moments and an added value in the happiest ones.

Last, but not least, I want to thank mathematical physics and in general

mathematics: it has given me one of my biggest passions in life developing my
sake for discovery and it made me understand that most everything in life has a
solution, if you sit there with constance and you look for it.

Bibliography

- [1] Gabriel Helmlinger, Paolo A. Netti, Hera C. Lichtenbeld, Robert J. Melder, and Rakesh K. Jain. *Solid stress inhibits the growth of multicellular tumour spheroids*. Nature Biotechnology Volume 15, August 1997.
- [2] C. Y. Chen, H. M. Byrne, J. R. King. *The influence of growth-induced stress from the surrounding medium on the development of multicell spheroids..* Journal of Mathematical Biology. 43, 191-220 (2001).
- [3] S. Astanin and L. Preziosi. *Multiphase Models of Tumour Growth*. Dipartimento di Matematica, Politecnico di Torino, Corso Duca degli Abruzzi 24, 10129, Torino, Italy.
- [4] M. A. J. Chaplain, B. D. Sleeman. *Modelling the growth of solid tumours and incorporating a method for their classification using nonlinear elasticity theory..* Journal of Mathematical Biology. (1993) 31:431-473.
- [5] Gang Cheng, Janet Tse, Rakesh K. Jain, Lance L. Munn. *Micro-Environmental Mechanical Stress Controls Tumour Spheroid Size and Morphology by Suppressing Proliferation and Inducing Apoptosis on Cancer Cells*. PLoS ONE | www.plosone.org | February 2009, Volume 4, Issue 2, e4632.
- [6] K.A. Landman, C.P. Please. *Tumour dynamics and necrosis: surface tension and stability*. IMA Journal of Mathematics Applied in Medicine and Biology (2001) **18**, 131-158.
- [7] Birbrair A, Zhang T, Wang ZM, Messi ML, Olson JD, Mintz A, Delbono O (July 2014). *Type-2 pericytes participate in normal and tumoral angiogenesis". American Journal of Physiology*. Cell Physiology. 307 (1): C25â€38.
- [8] Lozano G.M., Bejarano, I., Espino, J., Gonz alez, D., Ortiz, A., Garc a, J.F., Rodr nguez, A.B., Pariente, J.A. 2009). *Relationship between Caspase Activity and Apoptotic Markers in Human Sperm in Response to Hydrogen Peroxide and Progesterone*. Journal of Reproduction and Development 55(6): 615-621.
- [9] Catarina Br s-Pereira and Eduardo Moreno. *Mechanical Cell Competition*. Current Opinion in Cell Biology, available online at www.sciencedirect.com
- [10] Shraiman BI: *Mechanical feedback as a possible regulator of tissue growth*. Proc Natl Acad Sci U S A 2005, 102:3318-3323.

- [11] Alfio Grillo, Salvatore di Stefano, Airl Ramirez-Torres, Michele Loverre. *A study of growth and remodelling in isotropic tissues, based on the Anand-Aslan-Chester theory of strain-gradient plasticity*. GAMM 201900015. Dipartimento di Scienze Matematiche (DISMA), "G. L. Lagrange", Dipartimento di Eccellenza 2018-2022.
- [12] Salvatore Federico, Alfio Grillo, Shoji Imatani. *The linear elasticity tensor of incompressible materials*. *Mathematic and Mechanics of Solids* 2015, Vol. 20(6) 643-662.
- [13] Luigi Preziosi, Angiolo Farina.
On Darcy's law for growing porous media. *International Journal of Non-Linear Mechanics* 37 (2002) 485-491.
- [14] Greenspan, H.P.: *On the self-inhibited growth of cell cultures* *Growth*, 38, 81-95 (1974)
- [15] Helen Byrne, Luigi Preziosi.
Modelling solid tumour growth using the theory of mixtures.
Mathematical Medicine and Biology (2003) 20, 341-366
- [16] Margaret A. Knowles Peter J. Selby.
Introduction to the Cellular and Molecular Biology of Cancer
Oxford University Press.
- [17] Olive, P.L: and Durand, R.E. 1994. *Drugs and radiation resistance in spheroids: cell contact and kinetics*. *Cancer Metastasis Rev.*13:121-138.
- [18] Kobayashi, H., Man, S., Graham, C. H., Kapitain, S.J., Teicher, B.A., Kerbel, R.S., et al. 1993. *Acquired multicellular-mediated resistance to alkylating agents in cancer*. *Proc. Natl. Acad. Sci. USA* 90:3294-3298.
- [19] Continuum Mechanics notes, Academic Year 2016-2017, Polytechnic of Turin.